JOURNAL OF PETROLOGY | VOLUME 40 | NUMBER 5 | PAGES 729–754 | 1999

Diversity of Mafic Rocks in the Ronda Peridotite: Evidence for Pervasive Melt–Rock Reaction during Heating of Subcontinental Lithosphere by Upwelling Asthenosphere

CARLOS J. GARRIDO[1,2]* AND JEAN-LOUIS BODINIER[2]

[1]DP. MINERALOGIA Y PETROLOGIA, UNIVERSIDAD DE GRANADA, 18002 GRANADA, SPAIN

[2]ISTEEM, Lab. Tectonophysique, CNRS & UNIVERSITÉ DE MONTPELLIER II, CC 57, PLACE EUGÈNE BATAILLON, 34095 MONTPELLIER CEDEX 05, FRANCE

RECEIVED FEBRUARY 19, 1998; REVISED TYPESCRIPT ACCEPTED OCTOBER 9, 1998

On the basis of their structural and compositional characteristics, mafic rocks in the Ronda peridotite are classified into four groups: group A (garnet-bearing rocks) occurring in the spinel tectonite domain; group B (spinel websterites) along the recrystallization front; group C (Ti-rich spinel pyroxenites) in the granular tectonite and plagioclase tectonite domains; and group D (Cr-rich pyroxenites) as composite layers along the recrystallization front, dykes in the spinel tectonites, and single layers in the other domains. The spinel tectonite domain and group A layers represent the vestiges of an old, veined subcontinental lithosphere. The other mafic groups were formed during a later magmatic event that originated the present petrological zoning of the massif, and, in most cases, have replaced older mafic layers (groups B and D) or peridotites (group C). The magmatic event that led to the diversity and zoning of mafic layers was caused by melting of the base of thinned subcontinental lithosphere by upwelling asthenosphere, followed by infiltration of asthenospheric melts. The different groups of mafic layers record several stages of this event: (1) in the thermal climax, group B was formed at the expense of group A by melt–rock reactions at increasing melt mass. This stage was coeval with partial melting of the host lithospheric peridotites and the development of the recrystallization front; (2) upon cooling of the lithosphere, group C was formed by near-solidus, melt-consuming reactions between melt and peridotite at high melt/rock ratios. Group C parental melts were mixtures of partial melts of lithospheric peridotites and garnet pyroxenites, and alkaline melts infiltrated from the underlying asthenosphere; (3) in the waning stages of this magmatic event, group D was formed by magmatic replacement of group A, B and C layers by small-volume melt fractions that percolated pervasively throughout the massif and had a refractory, calc-alkaline character. Locally, these melts were tapped into cracks forming intrusive dykes.

KEY WORDS: *Ronda peridotite; mafic layers; pyroxenites; subcontinental lithospheric mantle*

INTRODUCTION

Layers, irregular bodies and dykes of mafic rocks, mainly pyroxenites, commonly occur in orogenic peridotite massifs. Mafic rocks crop out roughly parallel to the foliation of the host peridotites (e.g. Kornprobst, 1969, 1970; Dickey, 1970; Conquéré, 1977; Shervais, 1979) or, rarely, as cross-cutting dykes or veins (Conquéré, 1971; Wilshire *et al.*, 1980; Bodinier *et al.*, 1987*a*). Whereas most investigators agree on the magmatic origin of dykes and veins, there is some controversy about the origin and significance of the concordant mafic layers. They are often interpreted as high-pressure mineral segregates in magma conduits, with primary mineralogy and textures partly obscured by subsequent deformation and metamorphism. This interpretation is similar to the one proposed for mafic mantle xenoliths, and is generally

*Corresponding author. Present address: Université de Montpellier II, ISTEEM Lab. Tectonophysique, Cc 57, Place Eugéne Bataillon, 34095 Montpellier Cedex 05, France. Telephone: 33 467 143943. Fax: 33 467 143603. e-mail: garrido@babouin.dstu.univ-montp2.fr.

supported by experimental and geochemical evidence (Yoder & Tilley, 1962; O'Hara & Yoder, 1967; Frey & Prinz, 1978; Irving, 1980; Bodinier *et al.*, 1987*b*; Suen & Frey, 1987; Pearson *et al.*, 1993). As such, mafic layers have been used to investigate the geochemical composition of primary mantle melts and the mechanisms of melt segregation from partially molten peridotites (Obata *et al.*, 1980; Loubet & Allègre, 1982; Obata & Nagahara, 1987; Suen & Frey, 1987; Pearson *et al.*, 1993; Reisberg & Lorand, 1995). Together with pyroxenite dykes, they were also studied to constrain high-pressure fractional crystallization and/or reaction of upwelling melts with lithospheric peridotites (Bodinier *et al.*, 1987*a*, 1990; Downes *et al.*, 1991; Kumar *et al.*, 1996).

Alternatively, Allègre & Turcotte (1986) have interpreted the mafic layers as subducted oceanic crust, stretched and metamorphosed in the convective mantle. This hypothesis is based on the extreme diversity of their radiogenic isotopic compositions and the isotopic differences between pyroxenites and peridotites (Polvé & Allègre, 1980; Hamelin & Allègre, 1988). In a few cases, this hypothesis is supported by the trace element signature of pyroxenites, suggesting a low-pressure magmatic history (Pearson *et al.*, 1989; Kornprobst *et al.*, 1990). In this model, the orogenic massifs are considered as analogues for the source region of oceanic basalts, and the mafic layers the cause of the recycling isotopic and trace element signature in oceanic basalts (e.g. Prinzhofer *et al.*, 1989; Hauri, 1996; Hirschman & Stolper, 1996).

We present a combined field and geochemical study of mafic rocks from the Ronda massif which complements recent structural and geochemical investigations of the peridotites (Gervilla & Remaïdi, 1993; Remaïdi, 1993; Van der Wal & Vissers, 1993, 1996; Van der Wal & Bodinier, 1996). The Ronda peridotite (Southern Spain) contains a petrologically and geochemically diverse group of mafic rocks (Obata, 1980; Frey *et al.*, 1985; Suen & Frey, 1987). This diversity largely overlaps that of pyroxenite xenoliths in basalts (Wilshire & Shervais, 1975; Frey & Prinz, 1978; Kornprobst *et al.*, 1987). Our aim is to clarify the relationships between the different groups of mafic rocks and the structural and magmatic events recorded by the peridotites in this massif. These observations, together with the relative timing of emplacement, allow us to put constraints on the origin and meaning of Ronda mafic rocks.

GENERAL FEATURES OF THE RONDA PERIDOTITE

The Ronda peridotite is the largest (~300 km^2) of several ultramafic massifs located in the Betic Cordillera (Southern Spain) (Fig. 1). The Betic–Rifean orogenic belt, which also includes the Beni Bousera peridotite in Northern Morocco, is the westernmost segment of the Alpine belt in Europe (Fig. 1). Comprehensive reviews of the regional geology of the Ronda massif have been presented by Tubia (1994) and Vissers *et al.* (1995) among many others. Van der Wal & Vissers (1996) have discussed the different models proposed for the crustal emplacement of the massif.

A distinctive feature of the Ronda peridotite is the existence of a kilometre-scale petrological zoning (Dickey, 1970; Obata, 1980) (Fig. 1). Obata (1980) mapped the massif into four domains based on metamorphic facies and subfacies defined by the mineral assemblages of peridotites and mafic layers. From the northwestern to the southern and eastern parts of the massif, he distinguished a garnet lherzolite, a spinel lherzolite—divided into ariegite and seiland subfacies—and a plagioclase lherzolite domain (Fig. 1).

Van der Wal & Vissers (1996) distinguished three structural domains:

(1) The spinel tectonite domain is the oldest. It is located in the NW of the massif, in the area attributed by Obata to the garnet lherzolite facies and the ariegite subfacies (Fig. 1). This domain is composed of intensely foliated porphyroclastic spinel peridotites and mylonitic garnet–spinel peridotites, and includes minor amounts of garnet-bearing mafic layers.

(2) The younger granular peridotite domain roughly coincides with Obata's seiland subfacies. It is essentially composed of undeformed granular spinel peridotites and spinel-bearing mafic layers. This domain is well exposed in the central part of the Ronda peridotite and occupies most of the western part of the massif around the locality of Monte de los Reales (Fig. 1). On the basis of structural and petrological criteria, the granular domain can be further subdivided into three subdomains (Van der Wal & Bodinier, 1996). From NW to SE—and with decreasing relative age indicated by overprinting field relationships—these subdomains are: (a) coarse-grained granular peridotites, with abundant harzburgites; (b) fine-granular peridotites, mainly olivine-rich lherzolites; (c) a layered sequence of lherzolites, olivine-rich lherzolites, harzburgites and dunites.

(3) The plagioclase tectonite domain is the youngest of the three structural domains. This domain basically corresponds to Obata's plagioclase lherzolite facies (Fig. 1), and is composed of moderately foliated, porphyroclastic plagioclase peridotites. The development of the plagioclase tectonite domain is related to the crustal emplacement of the massif and overprints older magmatic and deformation structures observed in the other tectonic domains (Van der Wal & Vissers, 1996).

One of the most remarkable features of the Ronda massif is the transition from the spinel tectonites to the granular peridotite domain. Field and microstructural evidence indicates that recrystallization and grain growth

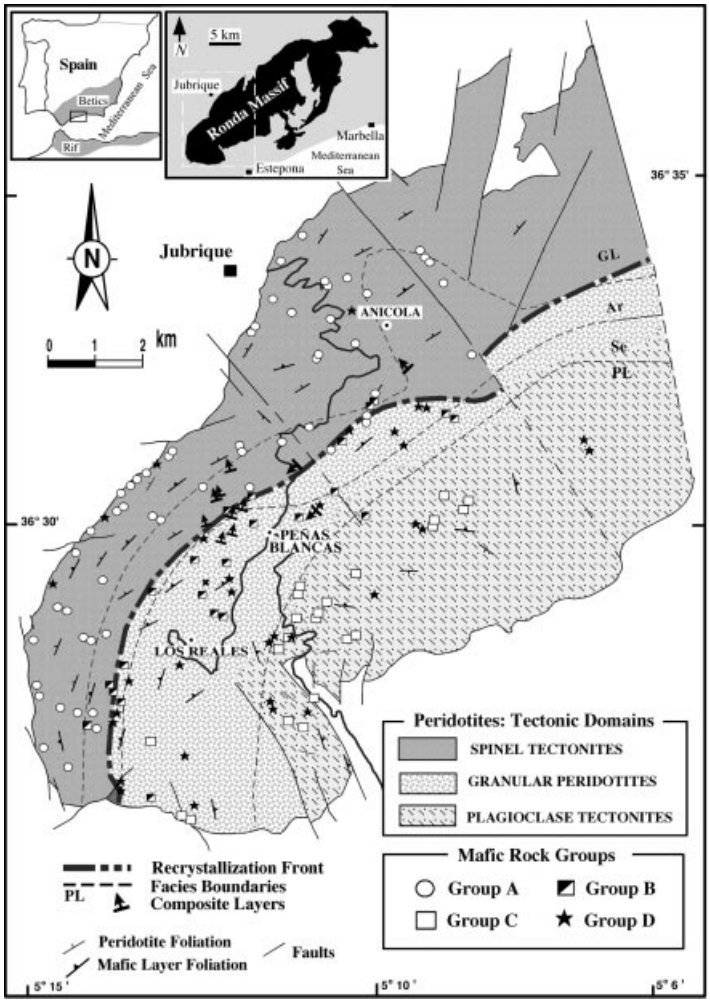

Fig. 1. Map of the western part of the Ronda peridotite massif showing the distribution of the different groups of mafic rocks distinguished in this study (Table 1). The arrows indicate the relative position of the older rock type in the composite layers, as deduced from structural and textural observations. Also shown are the tectonic and metamorphic domains and the recrystallization front mapped by Van der Wal & Vissers (1996), and the petrological facies boundaries mapped by Obata (1980). GL, garnet lherzolite facies; Ar and Se, ariegite and seiland subfacies, respectively, of the spinel lherzolite facies; PL, plagioclase lherzolite facies. Insets: location of the studied area within the realm of the Betic–Rifean orogenic belt (Southern Spain and Northern Morocco—left) and in the western Betic orogenic belt (Southern Spain—right).

occurred within a narrow transition zone, about 200 m wide, interpreted as a recrystallization front (Van der Wal & Vissers, 1993) (Fig. 1). Garrido *et al.* (1993) and Van der Wal & Bodinier (1996) argued that the recrystallization was related to kilometre-scale pervasive melt porous flow through the granular peridotites. Van der Wal & Bodinier (1996) concluded that the recrystallization front was formed by feedback processes between grain growth, porosity, and incipient melting of peridotites, during heating of lithospheric peridotites by upwelling asthenosphere. They interpreted this sharp front as a transition between a high melt-fraction domain (granular peridotite domain) pervasively equilibrated with basaltic melts, and a low melt-fraction domain (spinel tectonite domain) infiltrated by volatile-rich small volume melts.

CLASSIFICATION, FIELD OCCURRENCE AND PETROGRAPHY OF MAFIC ROCKS

Previous studies have classified Ronda mafic rocks into a 'magmatic-type' (Al-rich) and a 'tectonic-type' (Cr-rich) (Dickey, 1970; Obata *et al.*, 1980). However, this classification is somewhat misleading, especially for the spinel-bearing mafic rocks that commonly show transitional characteristics between these two types. On the basis of their current mineral assemblages (Table 1), structure (Fig. 2), texture (Fig. 3), chemical composition (Fig. 4), and the peridotite domain in which they occur (Fig. 1), we propose a classification of Ronda mafic rocks in four groups (A, B, C and D) (Table 1; see this table for mineral abbreviations and the mineral assemblage of

Table 1: Classification and general characteristics of Ronda mafic layers

Clas.	Current ass.	Primary ass.	Rock type	Domain	Structure	Microstructure
A	*Intermediate* ti-*number, low and variable* mg-*number, low* cr-*number*					
A1	cpx + grt + pl ± (rut, qtz, amp, gph) (pre- and syn-S_1)	cpx ± grt (gph, qtz) (pre-S_1)	Mafic garnet granulites	Exclusively ST	Strongly deformed layers (up to 6 m), often showing isoclinal folds and boudinage (Fig. 2a). Sharp contacts with wall-rock peridotites	Metamorphic: porphyroclastic or granoblastic. A1: porphyroclasts of grt and cpx (rare); recrystallized matrix of pl and cpx (Fig. 3a). A2: porphyroclasts of grt and cpx; recrystallized matrix of cpx, grt and opx (rare) (Fig. 3b)
A2	cpx + grt ± opx ± (rut, amp, pl, phl) (pre- and syn-S_1)	cpx ± grt (pre-S_1)	Garnet clinopyroxenites Garnet websterites (rare)	Exclusively ST	Foliation and lineation defined by grt and cpx. Some modal layering (cpx/pl) may occur. May occur in 'composite layers' (Fig. 2c and d)	In some cases, cpx shows extensive exsolution of grt and opx. (both groups): LPO and dynamic recrystallization in cpx; deformation lamellae in grt
B	*intermediate* ti-*number, high* mg-*number, intermediate* cr-*number*					
	opx + cpx + sp ± grt (pl, ol) (post-S_1)	group A assemblages	Spinel websterites Spinel–garnet websterites (rare)	Mostly along RF–GP (cgp)	Display isoclinal folds and boudinage, but no tectonic foliation. May occur in 'composite layers'	Coarse-grained cpx–opx–sp–pl clusters (former grt), aligned parallel to S_1 foliation (Fig. 3c and d). Evidence for strong annealing and recrystallization. Cpx shows inherited LPO
C	*High* ti-*number and* mg-*number, low to intermediate* cr-*number*					
C1	opx + cpx + sp ± pl ± (ol, amp, ilm) (post-S_1)	opx + cpx (± sp?) (pre-S_2)	Spinel websterites	GP (lgp) and PT	Rarely isoclinally folded or strongly deformed. Diffuse contacts with the enclosing peridotites. Resemblance to 'sill complexes' (Fig. 2b)	Magmatic, cumulate-like textures (Fig. 2f). Coarse opx and cpx showing pervasive exsolution of pyroxenes (also sp). Also kink bands. Where affected by S_2, display porphyroclastic textures
C2	opx + ol ± cpx ± sp ± pl ± amp ± ilm (post-S_1)	opx + ol ± cpx (± sp?) (pre-S_2)	Spinel olivine websterites Spinel orthopyroxenites	GP (lgp) and PT	Where affected by PT deformation (S_2), display foliation defined by cpx flattening, and sp and pl lineations	
D	*Very low* ti-*number, high* mg-*number and* cr-*number*					
D1	cpx + opx ± ol (post-S_1/pre-S_2)	cpx ± opx ± ol (post-S_1/pre-S_2)	Websterites (common) Olivine websterites Clinopyroxenites	Mainly GP (fgp, lgp) (rare) ST and PT	GP and PT: folded or straight layers (up to 6 m). Concordant relative to S_1	Magmatic textures coarse-grained opx and cpx (up to 6 cm). Olivine usually interstitial. No textural evidence for plastic deformation. Pervasive exsolution of opx in large cpx (up to 6 cm)
D2	opx + cpx + sp (± ol ± pl) (post-S_1/pre-S_2)	opx + cpx + sp ± ol (post-S_1/pre-S_2)	*Spinel websterites*	GP and PT	RF: Concordant 'composite layers' (relative to S_1) with group A or B rock types. ST: (rare) cross-cutting, intrusive dykes. Only D1 assemblages occur in dykes	Where affected by S_2, porphyroclastic textures with cpx showing kink bands and evidence for dynamic recrystallization of pyroxenes
D3	opx +(cpx ± ol) (post-S_1)	cpx + opx ± ol (post-S_1)	Orthopyroxenites	(rare)GP, PT and ST		Cumulate-like textures (Fig. 3e). Opx shows cpx exsolutions

Clas., proposed classification, in groups and subgroups, for Ronda mafic layers. Current Ass., current mineral assemblage. Primary Ass., primary assemblage as deduced from petrographic and chemical considerations. Mineral abbreviations: amp, amphibole; cpx, clinopyroxene; gph, graphite; grt, garnet; ilm, ilmenite; ol, olivine; opx, orthopyroxene; phl, phlogopite; pl, plagioclase; qtz, quartz; rut, rutile; sp, spinel. S_1, foliation of peridotites in the spinel tectonite domain; S_2, foliation of the peridotites in the plagioclase tectonite domain. Relation to the foliation as deduced from field and microscopic observations: pre-, pre-tectonic; syn-, syn-tectonic; post-, post-tectonic. Domain: Ronda tectonic domains and subdomains (Fig. 1). ST, spinel tectonite domain; RF, recrystallization front; GP, granular peridotite domain (GP subdomains: cgp, coarse-grained granular peridotites; fgp, fine granular peridotites; lgp, layered granular peridotites); PT, plagioclase tectonite domain.

each mafic group). These groups are well discriminated by three chemical indices (all in mol %): *mg*-number [100 × MgO/(MgO + ΣFeO)], *cr*-number [100 × $Cr_2O_3/(Cr_2O_3 + Al_2O_3)$] and *ti*-number [200 × $TiO_2/(2TiO_2 + Al_2O_3)$] (Fig. 4).

Group A

This group comprises greyish, garnet mafic granulites (subgroup A1) and dark grey garnet pyroxenite layers (subgroup A2), occurring exclusively in the spinel tectonite domain (Fig. 1). Group A includes the most differentiated rocks in Ronda, with *mg*-number displaying a wide range of values (55–80) (Fig. 4) similar to that found for Ronda mafic layers by Suen & Frey (1987). There is no correlation between *mg*-number and the spatial distribution of the samples in the spinel tectonite domain. Group A is also characterized by a restricted range of *ti*-number (3–15), negatively correlated with *mg*-number (Fig. 4). The clinopyroxenes have intermediate TiO_2 contents and the highest Al_2O_3 (especially subgroup A1) and Na_2O contents among Ronda mafic rocks (Table 2). Though extremely rare, graphite occurs as a subordinate phase (Obata, 1980). Graphite pseudomorphs after diamond have been reported in garnet pyroxenites from Ronda (Davies *et al.*, 1993).

Most often, group A mafic rocks occur as single layers (up to 5 m thick) with sharp contacts with wall-rock peridotites. The layers are straight and parallel to the foliation of the spinel tectonites, isoclinally folded, and/or boudinaged (Fig. 2a). The modal layering described in Beni Bousera garnet pyroxenites is rare, yet the garnet mafic granulites have a gneissic layered appearance as a result of plagioclase seams (Fig. 3a). Rarely, near the recrystallization front (Fig. 1), they occur as part of composite layers with group D mafic rocks (Fig. 2c and d). Group A mineralogy, mineral compositions and textures are of metamorphic origin (Fig. 3a and b). The rocks display microstructural evidence for substantial plastic deformation, such as lattice preferred orientation (LPO) and dynamic recrystallization of pyroxenes (Fig. 3b), and flattening of garnets parallel to the spinel tectonite foliation (Fig. 3a and b).

Group B

This group is composed of dark greenish spinel websterites and, rarely, spinel–garnet websterites. They mainly occur along the recrystallization front and sporadically in the coarse-granular subdomain (Fig. 1). Group B mafic rocks generally have higher *mg*-number (77–90) and *cr*-number (up to 7) than group A (Fig. 4). This observation indicates that significant changes in the composition of mafic layers occur across the recrystallization front. Group B clinopyroxenes are Al_2O_3 rich, but have higher MgO and Cr_2O_3, and lower Na_2O contents than group A clinopyroxenes (Table 2).

Group B mafic rocks occur as single layers or form composite layers with group D websterites. Similar to group A, group B layers show strongly deformed field structures, such as boudinage and isoclinal folding. Although generally hosted by non-foliated peridotites, the layers are parallel to foliation and layering of the spinel tectonite domain (Van der Wal & Vissers, 1996). In contrast with field structures, the microstructures are seemingly undeformed. They are typically granular, with large pyroxenes (up to 3 cm) and coarse cpx–opx–sp–pl clusters (Fig. 3d). Several observations indicate that these clusters result from breakdown of former garnets. For instance, in group B spinel–garnet websterites, relics of garnet (now replaced by kelyphite) are rimmed by coarse cpx–opx–sp–pl aggregates produced by garnet breakdown (Fig. 3c). These rim aggregates are comparable with the clusters found in group B spinel websterites (Fig. 3d). In both rock types, the cpx–opx–sp–pl aggregates are aligned parallel to the foliation of the spinel tectonite domain and mimic the structure observed for garnet in group A layers (Fig. 3c and d). This indicates that group B pyroxenites were formed at the expense of former group A layers, a process that was associated with substantial grain growth, annealing of the former deformation microstructures and whole-rock chemical changes. These changes are comparable with those registered by the peridotites across the recrystallization front (Van der Wal & Bodinier, 1996). These observations point to an open-system process whereby group A layers were replaced by spinel–plagioclase-bearing assemblages (group B) during the magmatic event inferred for the development of the recrystallization front.

Group C

This group comprises layers of brownish spinel websterites and olivine–spinel websterites (Table 1), which were classified as olivine gabbros in previous studies (Obata, 1980; Suen & Frey, 1987). As plagioclase is of metamorphic origin, we prefer to classify them as websterites. They mostly occur in the layered-granular subdomain (Remaïdi, 1993) and throughout the plagioclase tectonite domain (Fig. 1). They are characterized by high *mg*-number, with a narrow variation range (77–87), and are clearly distinguished from the other Ronda mafic rocks by their higher *ti*-number for a given *mg*-number value (Fig. 4). The clinopyroxenes display high MgO content and the highest TiO_2 contents among Ronda mafic layers (Table 2).

In the field, group C layers are distinguished from all the other Ronda mafic layers by the lack of significant deformation, except for some open folds coeval with the

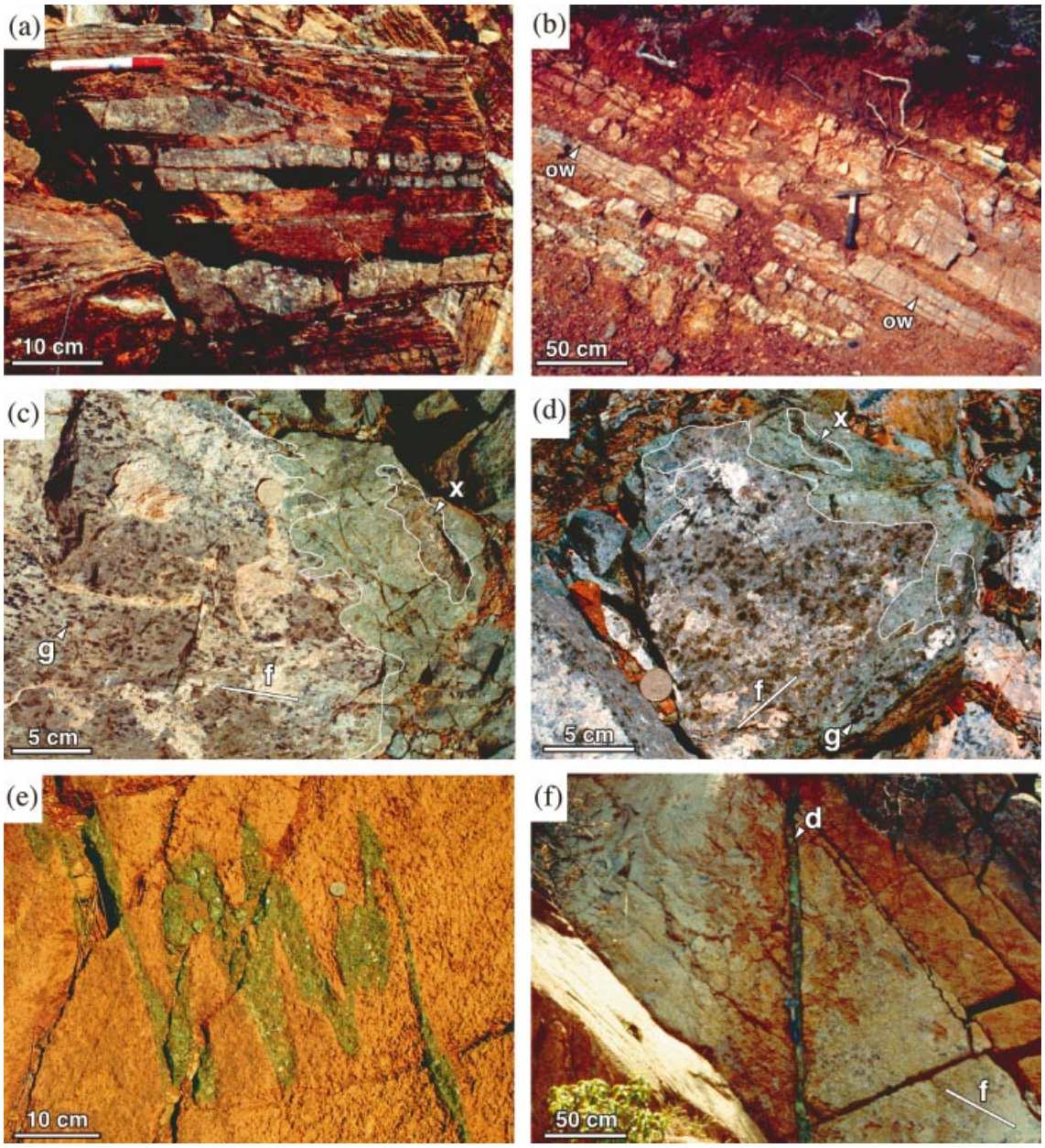

Fig. 2. Representative outcrops of mafic rocks in the Ronda peridotite. (a) Isoclinal folds of garnet pyroxenites and garnet mafic granulites (group A) interlayered with spinel peridotite mylonites from the spinel tectonite domain. (b) Typical outcrop of layered spinel websterites (group C)—enclosed by harzburgites and dunites—in the plagioclase tectonite domain. Spinel websterite layers grade along strike into olivine websterites (ow), harzburgites and/or dunites. The olivine websterites contain elongated, millimetre-thick olivine flames interpreted as relics of the host peridotite. (c and d) Details of a composite layer (~5 m thick) near the locality of Puerto de Peñas Blancas (see Fig. 1), slightly to the north of the recrystallization front. This layer is composed of two distinct rock types: one side (the left side in both figures) is composed of highly deformed, garnet mafic granulite (group A) with large garnet porphyroclasts (g) aligned parallel (f) to the foliation of the host peridotite; the other side (the right side) is composed of chromium websterites (group D) with coarse, seemingly undeformed, 'cumulate'-like textures. The latter rock type contains 'xenoliths' (x) of garnet mafic granulites, partially replaced by orthopyroxenite. The relic foliation in these xenoliths can be traced back into the garnet granulite side of the composite layer. This structure indicates that the garnet mafic granulite protolith was metasomatically replaced by chromium websterite. It should be noted that the transition between the two rock types (outlined by a white line) is sharp and oblique to the foliation of the garnet granulite. (e) Isoclinal folds of seemingly undeformed, very coarse-grained chromium websterite (subgroup D1) within coarse-grained harzburgites from the granular peridotite domain. (f) Intrusive dyke (d) of chromium websterite (group D) cutting the foliation of the spinel tectonites (f) at high angle.

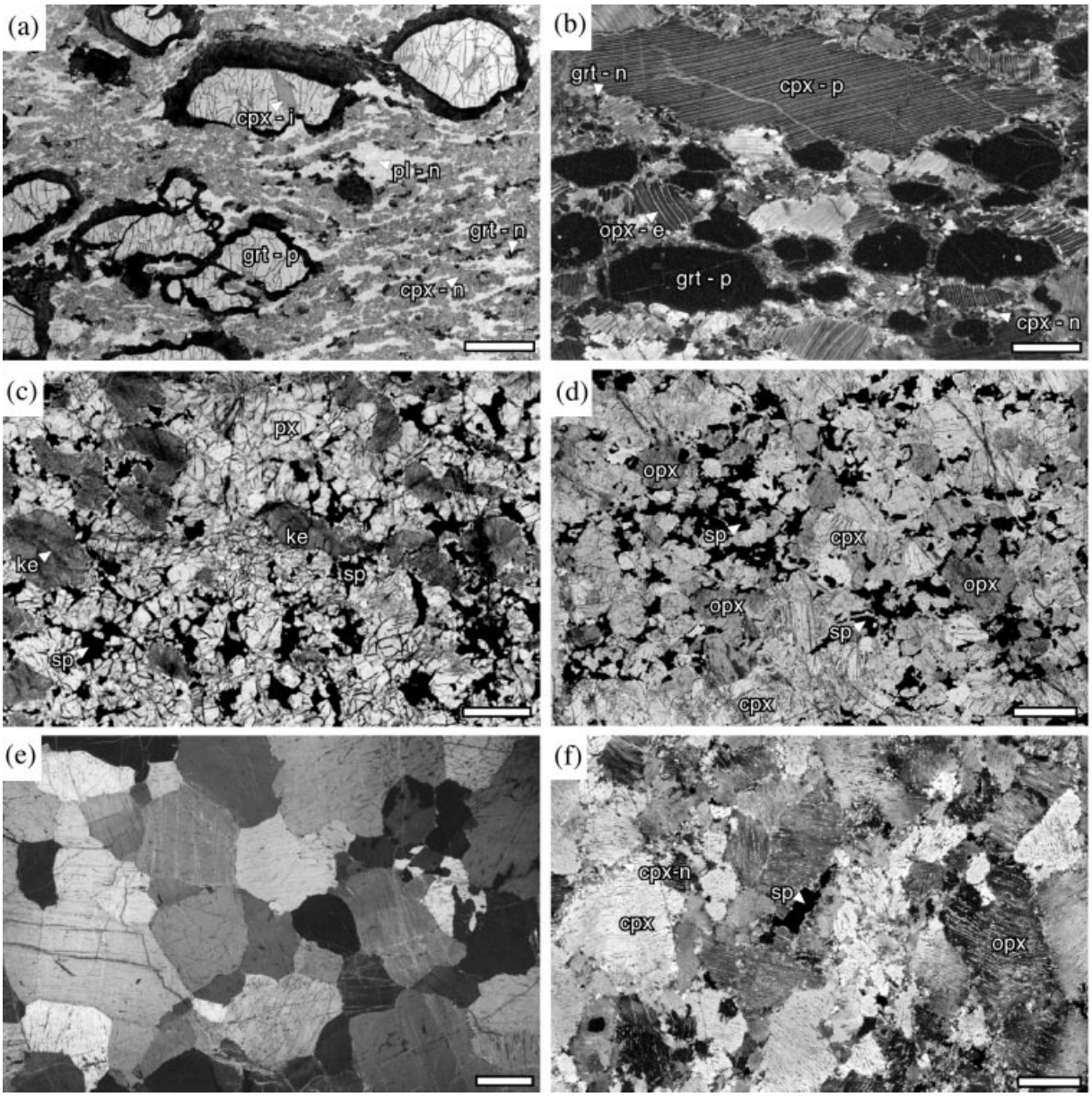

Fig. 3. Microphotographs of representative microstructures of Ronda mafic rocks. (a) Highly deformed garnet mafic granulite (subgroup A1) in the spinel tectonite domain. This rock shows a porphyroclastic microstructure made up of garnet porphyroclasts (grt-p), partially replaced by kelyphite (black coronas around garnet), in a fine-grained matrix of plagioclase (pl-n), clinopyroxene (cpx-n), and garnet (grt-n) neoblasts. Garnet generally contains inclusions of undeformed clinopyroxene (cpx-i). Garnet porphyroclasts and seams of plagioclase neoblasts define a foliation parallel to that of the host peridotite (plane-polarized light; PPL). (b) Highly deformed garnet clinopyroxenite (subgroup A2) in the spinel tectonite domain. This rock displays a porphyroclastic microstructure made up of large porphyroclasts of clinopyroxene (cpx-p) [with exsolved orthopyroxenes (opx-e) ± garnets] and garnet (grt-p), in a fine-grained matrix of clinopyroxene (cpx-n) and garnet (grt-n) neoblasts (crossed-polarized light; XPL). (c) Granular microstructure in a garnet–spinel websterite (group B) near the recrystallization front. Relics of garnet, now totally replaced by kelyphite (ke), are aligned parallel to the foliation of the spinel tectonites. Garnet is surrounded by coarse-grained aggregates of Al-spinel (sp), clinopyroxene and orthopyroxene (both marked as 'px'). This assemblage is interpreted as a transient assemblage produced by magmatic breakdown of garnet during melt–rock reactions (PPL). (d) Granular microstructure in a spinel websterite (group B) of the granular domain. This rocks is devoid of garnet (or kelyphite), which has been completely transformed into coarse-grained clusters of Al-spinel (sp), orthopyroxene (opx) and clinopyroxene (cpx). The matrix is composed of coarse-grained clinopyroxene (cpx). Clusters are aligned parallel to the foliation of the spinel tectonites [see (b)]. This assemblage is interpreted as the result of complete magmatic breakdown of previous garnet-bearing rocks (PPL). (e) Coarse-grained, cumulate-like microstructure in an orthopyroxenite (subgroup D3) of the granular peridotite domain (XPL). (f) Coarse granular microstructure in a spinel websterite (group C) of the plagioclase tectonite domain. The microstructure is defined by coarse clinopyroxenes (cpx), orthopyroxenes (opx), and Al-spinel (sp) partly transformed into plagioclase. Some static recrystallization of clinopyroxene (cpx-n) and orthopyroxene occurred along grain boundaries (XPL). Scale bar represents 1 mm; all micrographs are from sections perpendicular to the foliation—and parallel to the lineation—of the spinel tectonite domain.

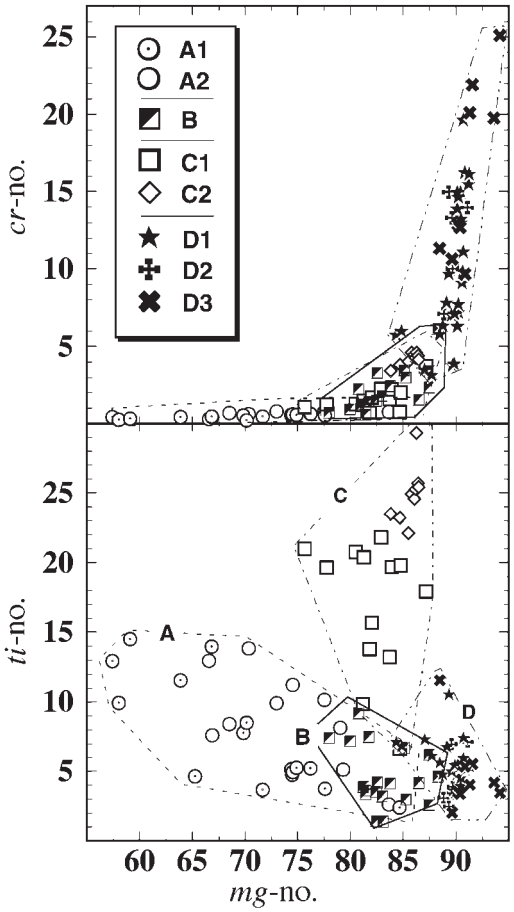

Fig. 4. Plots of *cr*-number {= 100 × [Cr_2O_3/(Cr_2O_3 + Al_2O_3)] mol %} and *ti*-number {= 200 × [TiO_2/(2 × TiO_2 + Al_2O_3)] mol %} vs *mg*-number {= 100 × [MgO/(MgO + FeO)] mol %} for the Ronda mafic rocks. Compositional fields are shown for the main mafic rock groups (A, B, C and D). The symbols identify the subgroups of mafic layers (see Table 1).

development of the plagioclase tectonite domain (Van der Wal & Vissers, 1996). They typically occur as swarms of straight layers, or elongated lenses, hosted by harzburgites and dunites (Fig. 2b) (Remaïdi, 1993). In that sense, group C outcrops resemble sill-complexes described in the transition zone of some ophiolites (e.g. Boudier & Nicolas, 1995). Individual layers and lenses display a poor to well-developed modal banding defined by variations of the olivine/pyroxene ratio at different scales (from a few millimetres to several centimetres) (Fig. 2b). The outcrops show gradual transitions—both across layering and along strike—from peridotites containing thin and rather diffuse pyroxene layers (<1 cm) to thick websterite lenses (>1 m) containing thin olivine seams. Field observations, as well as petrographic observations showing development of secondary pyroxene after olivine (Remaïdi, 1993), indicate that the olivine seams derive from the host peridotite. These features demonstrate that group C layers do not represent 'sill-cumulates' precipitated in open magma conduits, but they were formed by replacement of peridotites via pyroxene-forming melt–rock reactions. Burg *et al.* (1998) proposed a similar process for the origin of mantle websterites at the base of the obducted Kohistan arc (Northern Pakistan).

Group D

This group is composed of bright green clinopyroxenites, websterites and olivine websterites (subgroup D1), spinel websterites (subgroup D2), and scarce, light brown orthopyroxenites (subgroup D3) (Table 1). These rocks have been referred to as 'tectonic-type' in previous studies (Dickey, 1970). They are characterized by high and relatively constant *mg*-number values (85–94) and are distinguished from the other Ronda mafic rocks by higher *cr*-number (3–25) (Fig. 4). They contain bright green clinopyroxenes with very low Al_2O_3 and TiO_2, and very high Cr_2O_3 and MgO contents (Table 2).

Detailed mapping shows that group D pyroxenites are more common in Ronda than suggested by earlier works (Obata, 1980). Their abundance and field structure vary according to the tectonic domains (Fig. 1):

(a) The plagioclase tectonites and the fine- and layered-granular subdomains contain about 90% of group D occurrences (single layers; ~3 cm to 6 m thick). Similar to group A and B, group D layers display deformed field structures, such as isoclinal folding (Fig. 2e), and their orientation is concordant with the spinel tectonite structures. However, they have coarse-grained granular textures comparable with that of magmatic cumulates (Fig. 3e), with clinopyroxenes (up to 5 cm) showing pervasive exsolution of orthopyroxene. Plastic deformation microstructures are rarely observed.

(b) Along the recrystallization front, group D pyroxenites form 'composite layers' together with group A and B mafic rocks (Fig. 1). The most typical composite layers are characterized by an asymmetrical mineralogical and compositional zoning, with garnet-bearing rocks on one side and group D rock types on the other. An exceptional occurrence (6 m thick) is observed near the locality of Puerto de Peñas Blancas (Fig. 2c and d). This composite layer of garnet mafic granulite (subgroup A1) and websterite (subgroup D1) shows a sharp, irregular transition between these two rock types. The transition is marked by disappearance of garnet and plagioclase, and a substantial increase of pyroxene grain size (from a few millimetres up to 4 cm). The garnet granulite side is similar to the single layers of mafic granulites (subgroup A1) in the spinel tectonite domain. It is characterized by a fine-grained, porphyroclastic texture indicative of

extensive plastic deformation. In contrast, the websterite shows undeformed, coarse-grained microstructure comparable with that of other group D websterites in the granular domain. Embedded in the undeformed, coarse-grained websterite, there are irregular 'xenoliths' (1–20 cm) of deformed garnet granulite, locally replaced by orthopyroxenite (Fig. 2c and d). Foliation within the xenoliths is parallel to that of the garnet granulite side of the layer (Fig. 2c and d). Other outcrops show isoclinally folded layers of garnet-bearing rocks irregularly replaced by group D websterites. This observation indicates the magmatic replacement of group A layers in a late evolutionary stage of Ronda, after the deformation event recorded in the spinel tectonites.

(c) In the spinel tectonite domain, group D mafic rocks are scarce. They occur as intrusive websterites dykes (displaying only subgroup D1 assemblages) up to 10 cm thick, cross-cutting the foliation of the spinel tectonites at high angle (Fig. 2f). Less often, they occur as seams or narrow rims at the edge of group A layers (mostly subgroups D1 and D3).

WHOLE-ROCK AND TRACE ELEMENT CHEMISTRY

Sampling and analytical procedures

Large samples of mafic layers were crushed and ground in an agate mill. X-ray fluorescence (XRF) analyses of major elements and minor transition elements (V, Cr, Co, Ni, Cu, Zn) were performed at the Universities of Leeds (UK) and Granada (Spain). Selected samples were analysed for rare earth elements (REE) and other trace elements (Rb, Ba, Sr, Zr, Hf, Nb, Ta, Th, U, Pb) by inductively coupled plasma mass spectrometry (ICP-MS) at the University of Montpellier (France). The ICP-MS procedure, precision and accuracy have been reported by Ionov *et al.* (1992) and Garrido (1995). Representative analyses are given in Table 3. The entire dataset can be found in the *Journal of Petrology* on-line electronic database, at http://www.oup.co.uk/petroj/?f8.

Major elements

The Ronda mafic rocks display a wide range of *mg*-number values (57–94) which includes almost the entire range of pyroxenites from lherzolite massifs and ophiolites, and that of basalt-borne, mafic mantle xenoliths (Fig. 5). As a group, the Ronda mafic rocks show a large dispersion of major element abundances vs *mg*-number (Fig. 5). This dispersion has been previously noted in pyroxenites from massifs and xenoliths (Frey, 1980; Bodinier *et al.*, 1987*b*; Suen & Frey, 1987; Pearson *et al.*, 1993). Compared with basalts, they are strongly depleted in P_2O_5 and K_2O, whose concentrations are mostly below the XRF detection limit (0·02 wt %; Table 3).

Group A samples have relatively high Al_2O_3 and Na_2O, and low MgO contents (Fig. 5), especially subgroup A1, which contains 13–17·5 wt % Al_2O_3, 0·9–1·9 wt % Na_2O and 9–13 wt % MgO. Group A includes the most differentiated mafic rocks, with five samples having *mg*-number $\leq$65. Similar evolved compositions are found

Table 2: Electron microprobe analyses of clinopyroxenes from mafic rocks

Group:	A		B	C		D		
Subgroup:	A1	A2	B	C1	C2	D1	D1	D2
Sample:	RC51	RC159	RO314	RO102	RO122	RC75	RC28E	RO138
wt %								
SiO_2	50·19	51·94	48·86	48·93	48·52	52·38	51·25	51·23
TiO_2	0·37	0·90	0·62	1·20	1·99	0·09	0·07	0·20
Al_2O_3	10·14	8·38	8·14	7·46	8·91	4·59	5·51	5·89
Cr_2O_3	0·10	0·07	0·35	0·21	0·47	2·33	0·82	0·98
MgO	12·30	12·25	14·07	15·20	13·85	15·39	15·65	15·69
ΣFeO	4·34	6·20	4·63	4·86	3·45	1·96	2·70	2·49
MnO	0·1	0·1	0·2	0·1	0·1	0·1	0·1	0·2
CaO	20·91	17·36	22·17	21·36	20·83	21·93	23·34	22·22
Na_2O	1·67	2·72	0·92	0·54	1·20	1·48	0·65	0·77
Σ	100·08	99·93	99·92	99·90	99·34	100·22	100·12	99·64

See Table 1 for classification of mafic rocks. Analyses are for averaged core compositions. Analyses conducted at ISTEEM (Université de Montpellier II, France) electron probe regional facility.

Table 3: Representative whole-rock major and trace element analyses of Ronda mafic layers

	Group A (A1)			Group A (A2)			Group B			
Sample	RC104	RC100	RC149	RC157A	RC159	RO175	RO312B1	RC153–4/2	CAC2C	RC137C2
wt %										
SiO_2	47·09	48·57	48·48	46·48	46·74	47·98	51·79	47·90	51·11	41·90
TiO_2	0·80	0·95	0·89	0·46	0·77	0·31	0·13	0·18	0·18	0·16
Al_2O_3	13·83	14·40	14·18	14·36	12·26	14·75	6·95	10·89	6·31	9·68
Fe_2O_3	13·92	12·52	10·00	12·78	12·35	7·39	6·27	7·92	6·00	10·68
MnO	0·24	0·19	0·15	0·30	0·22	0·09	0·14	0·14	0·13	0·15
MgO	9·48	9·14	10·16	13·04	14·81	14·31	23·82	20·61	16·98	25·45
CaO	12·66	12·42	14·45	11·65	10·71	13·37	9·76	11·28	16·70	7·80
Na_2O	1·62	1·88	1·67	1·52	1·37	1·08	0·38	0·55	0·95	0·31
K_2O	0·02	<0·02	<0·02	<0·02	<0·02	0·04	<0·02	<0·02	<0·02	<0·02
P_2O_5	0·02	0·02	0·02	<0·02	0·02	0·04	<0·02	<0·02	<0·02	<0·02
LOI	0·00	0·00	0·00	0·00	0·25	0·00	0·00	0·12	0·92	2·85
Σ	99·68	100·10	100·01	100·60	99·51	99·36	99·24	99·59	99·28	98·99
mg-no.	57·43	59·12	66·81	66·90	70·37	79·32	88·27	83·75	84·86	82·52
ppm										
Sc	51	44	37	46	42	31	36	20	33	24
V	490	341	250	302	316	118	128	102	242	104
Cr	252	312	557	458	685		4593	2651	4082	3433
Co	56	51	43	59	62	79	51	73	39	104
Ni	83	119	198	306	437	328	616	608	409	1370
Cu			119	78	66	75	7	30		
Zn			59	62	47	37	33	34		
Rb	2·85	1·54	0·54	0·54	1·89	1·48	0·437	0·59	0·499	1·41
Sr	17·0	25·8	35·3	21·0	34·9	69·3	30·9	13·6	19·9	30·6
Zr	16	24	24	14	24	13	5·0	3·0	3·8	2·1
Nb	0·07	0·046	0·06	0·07	0·11	0·18	0·11	0·12	0·10	0·07
Ba	7·4	1·83	5·8	6·5	11·9	3·07	10·7	2·07	1·63	1·43
La	<d.l.	<d.l.	<d.l.	0·146	0·67	0·58	0·364	0·203	0·234	0·0448
Ce	0·1	0·3	0·3	0·6	2·3	1·8	1·4	1·3	0·8	0·3
Pr	0·082	0·209	0·206	0·170	0·492	0·336	0·266	0·233	0·175	0·081
Nd	0·8	1·8	1·8	1·2	3·1	1·9	1·6	1·3	1·1	0·5
Sm	1·22	1·68	1·49	0·75	1·47	0·73	0·55	0·354	0·57	0·280
Eu	0·57	0·78	0·63	0·349	0·62	0·352	0·197	0·180	0·222	0·132
Gd	3·39	3·41	2·23	1·59	2·56	1·11	0·67	0·388	0·92	0·379
Tb	0·77	0·68	0·378	0·365	0·52	0·197	0·116	0·067	0·177	0·063
Dy	5·94	4·67	2·47	2·99	3·83	1·36	0·79	0·434	1·21	0·435
Ho	1·39	1·01	0·498	0·73	0·86	0·286	0·175	0·087	0·263	0·089
Er	4·33	2·94	1·45	2·40	2·65	0·79	0·475	0·246	0·69	0·260
Tm	0·67	0·433	0·204	0·371	0·398	0·117	0·074	0·0352	0·101	0·0394
Yb	4·39	2·78	1·31	2·55	2·64	0·73	0·436	0·218	0·57	0·240
Lu	0·73	0·449	0·205	0·418	0·424	0·118	0·073	0·0358	0·092	0·0421
Hf	0·77	0·96	0·99	0·464	0·86	0·440	0·201	0·117	0·177	0·103
Ta	0·0051	0·0033	0·0056	0·0035	0·0059	0·0096	0·0066	0·0065	0·0036	0·0025
Pb	6·5	0·88	0·43	<0·30	0·71	<0·30	0·31	<0·30	0·66	
Th	0·008	0·0029	0·0029	0·0024	0·024	0·015	0·025	0·009	0·017	0·0041
U	<0·0020	0·0021	<0·0020	<0·0020	0·0043	0·0053	0·0030	0·0029	0·0054	<0·0020

	Group C (C1)			Group C (C2)		Group D (D1)			(D2)	Group D (D3)		
Sample:	RO3	RC118	RO102	R0300	R0301	RC75 (dyke)	RC68	RC71C	RC150A	RC161	RC176	RC170
wt %												
SiO_2	48·80	42·95	48·22	48·94	47·64	54·15	53·88	53·63	48·71	53·43	54·56	55·38
TiO_2	1·02	0·95	0·58	0·71	0·69	0·10	0·08	0·08	0·18	0·04	0·07	0·06
Al_2O_3	10·24	15·31	9·80	5·92	5·84	4·08	3·87	3·49	6·27	5·23	3·18	2·65
Fe_2O_3	9·30	7·28	8·23	8·04	8·43	4·81	4·75	3·65	4·89	6·93	6·57	5·99
MnO	0·16	0·16	0·15	0·15	0·15	0·10	0·12	0·11	0·11	0·13	0·12	0·13
MgO	20·32	16·54	21·29	23·31	26·12	23·71	23·88	19·13	25·24	30·32	33·11	32·91
CaO	8·98	12·70	9·75	11·88	10·12	10·47	11·64	18·64	10·00	2·60	0·88	1·69
Na_2O	1·02	0·99	0·74	0·59	0·51	0·61	0·36	0·42	0·63	0·06	0·05	<0·02
K_2O	<0·02	<0·02	<0·02	<0·02	<0·02	<0·02	<0·02	<0·02	<0·02	<0·02	<0·02	<0·02
P_2O_5	0·02	<0·02	0·02	<0·02	<0·02	<0·02	<0·02	<0·02	<0·02	<0·02	<0·02	<0·02
LOI	0·02	2·62	0·01	0·00	0·00	0·80	0·63	0·30	2·82	1·08	0·55	0·18
Σ	99·88	99·50	98·79	99·54	99·50	98·83	99·21	99·45	98·85	99·82	99·10	99·00
mg-no.	81·23	81·82	83·67	85·17	85·99	90·71	90·87	91·21	91·09	89·65	90·89	91·58
ppm												
Sc	30	52	34	35	34	33	24	33	36	14	8	14
V	173	235	275	232	222	213	124	148	179	118	104	114
Cr	1525	968	1550	2118	2304	10196	7629	6518	10631	6354	3495	7591
Co	64	39	60	63	76	48	37	25	62	88	84	81
Ni	900	363	775	1145	1337	1386	686	495	1508	835	1489	887
Cu	86		51	128	114	36	8	7	145	13	2·0	
Zn	64		58	47	47	62	31	25	36	44	48	34
Rb	0·215	2·43	0·097	0·214	0·090	1·17	0·125	0·167	0·493	0·85	0·147	0·055
Sr	54·1	30·5	22·0	53·0	45·0	18·3	6·3	8·9	20·7	21·4	1·26	0·452
Zr	50	24	14	13	12	8	0·9	1·1	8	0·6	1·1	0·20
Nb	0·06	0·043	0·09	0·013	0·012	0·031	0·08	0·08	0·11	0·06	0·026	0·025
Ba	0·81	7·0	<0·3	0·34	0·38	30·1	1·00	1·12	1·14	33·7	0·93	1·02
La	1·28	0·270	0·356	0·60	0·484	1·21	0·067	0·101	0·268	<d.l.	<d.l.	<d.l.
Ce	6·2	1·2	1·6	2·7	2·3	4·8	0·3	0·4	0·8	0·05	0·1	0·02
Pr	1·23	0·51	0·355	0·58	0·497	0·90	0·053	0·076	0·180	0·0102	0·0115	0·0052
Nd	7·1	4·1	2·4	3·7	3·1	5·0	0·3	0·5	1·2	0·1	0·1	0·03
Sm	2·35	2·44	1·09	1·45	1·25	1·59	0·167	0·226	0·53	0·0317	0·0310	0·0107
Eu	0·86	1·12	0·437	0·56	0·500	0·368	0·070	0·092	0·228	0·0138	0·0116	0·0056
Gd	2·91	4·13	1·73	1·93	1·71	1·17	0·274	0·365	0·85	0·052	0·0453	0·0280
Tb	0·480	0·72	0·320	0·313	0·278	0·130	0·055	0·073	0·158	0·0101	0·0087	0·0066
Dy	3·14	4·64	2·24	1·89	1·75	0·63	0·412	0·52	1·10	0·082	0·068	0·059
Ho	0·65	0·90	0·486	0·350	0·334	0·118	0·094	0·119	0·233	0·0182	0·0176	0·0164
Er	1·74	2·29	1·33	0·85	0·82	0·323	0·282	0·329	0·67	0·058	0·064	0·058
Tm	0·254	0·306	0·193	0·111	0·104	0·0449	0·0418	0·0489	0·097	0·0092	0·0116	0·0110
Yb	1·61	1·77	1·25	0·63	0·60	0·282	0·263	0·293	0·60	0·061	0·087	0·082
Lu	0·256	0·269	0·198	0·093	0·087	0·0427	0·0431	0·0477	0·099	0·0112	0·0172	0·0158
Hf	1·72	1·12	0·67	0·73	0·66	0·381	0·054	0·057	0·271	0·0235	0·0423	0·0095
Ta	0·0199	0·0037	0·0090	0·0024	0·0022	0·0010	0·0026	0·0020	0·0132	0·0043	0·0020	0·0019
Pb	<0·30	<0·30	<0·30	<0·30	5·4	2·20	0·57	2·15	<0·30	<0·30	0·45	<0·30
Th	0·006	<d.l.	0·007	0·0011	0·0014	0·061	0·011	0·013	0·008	0·0037	0·007	0·005
U	<0·0020	<0·0020	0·0025	<d.l.	<d.l.	0·0276	0·002	0·0029	<0·0020	<0·0020	<0·0020	<0·0020

LOI, loss on ignition; <d.l., below detection limit; blank, non-analysed; *mg*-number = 100 × [MgO/(MgO + ΣFeO)] in mol %. Major elements, V, Cr, Co, Ni, Cu and Zn analysed by XRF. Other trace elements analysed by ICP-MS. For ICP-MS analyses, the number of significant digits is calculated after detection limits reported by Garrido (1995).

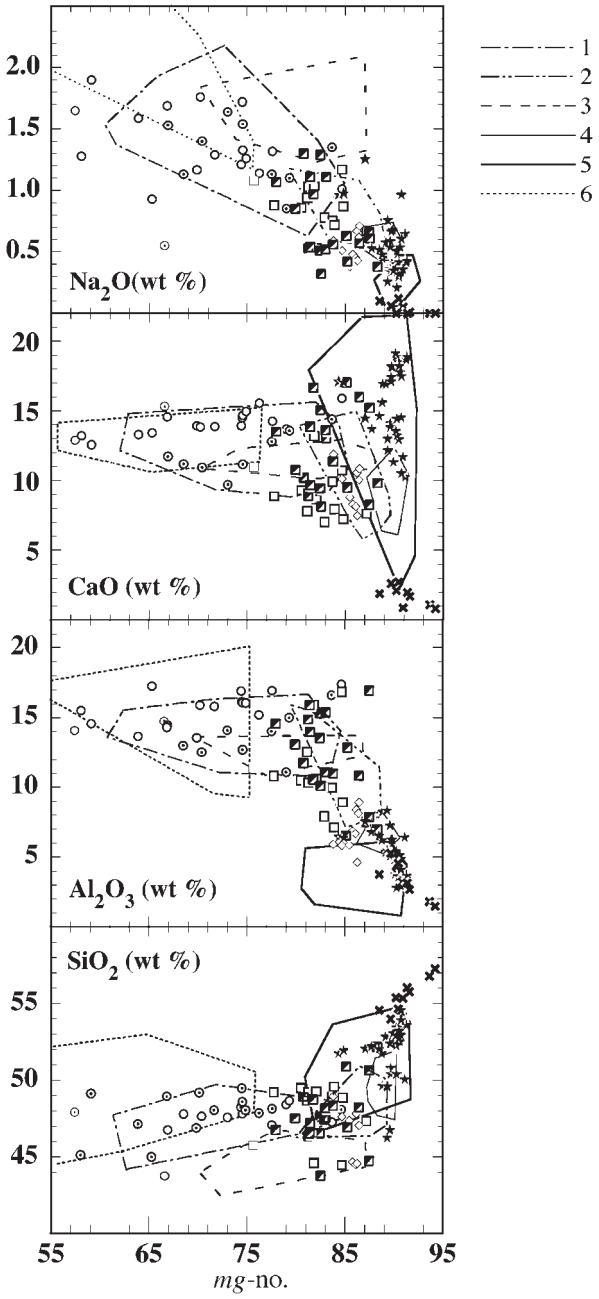

Fig. 5. Variation diagrams of Na_2O, CaO, Al_2O_3 and SiO_2 (wt %) vs *mg*-number for the Ronda mafic rocks. Symbols of rock types as in Fig. 4. The following compositional fields are shown for comparison: 1, 42 garnet pyroxenites from the Beni Bousera peridotite massif (Northern Morocco; Pearson *et al.*, 1993); 2, 20 garnet websterites and ariegites from the Ariège peridotite massifs (Pyrenees, Southern France; Bodinier *et al.*, 1987*a*); 3, 16 amphibole–garnet pyroxenites and 'lherzites' (hornblendite veins) from the Ariège peridotite massifs (Bodinier *et al.*, 1987*b*); 4, four spinel websterites from the Lanzo peridotite massif (Northern Italy; Bodinier, 1989); 5, 27 websterites from the mantle section of ophiolites from New Caledonia (J. L. Bodinier *et al.*, unpublished data, 1998) and Thailand (Orberger *et al.*, 1995); 6, 12 xenoliths of garnet mafic granulites in alkaline basalts from Victoria (Australia) (Griffin *et al.*, 1985).

in garnet pyroxenites from the Beni Bousera massif and in some granulite xenoliths from alkali basalts (Fig. 5).

In contrast with group A, group D is characterized by low Al_2O_3 (1·5–8·5 wt %), very low TiO_2 (0·03–0·24 wt %) and high MgO contents (18–35 wt %). This group is also distinguished by high, and relatively constant, *mg*-number values (87–94). CaO and SiO_2 contents are variable, reflecting modal variations of primary clinopyroxene, orthopyroxene and olivine. Compositions similar to group D are observed in pyroxenites from the mantle section of back-arc ophiolites (Fig. 5) and arc complexes (e.g. DeBari & Sleep, 1991).

Except for TiO_2, the compositions of groups B and C are intermediate between those of groups A and D. Group C is significantly more enriched in TiO_2 (up to 1·2 wt %) than is group B (up to 0·5 wt %) (Table 3). For most elements, groups B and C are comparable with layered pyroxenites from other lherzolite massifs (Fig. 5).

Minor transition elements

Group A mafic rocks have relatively low Cr abundances (250–1200 ppm) and *cr*-number values (≤ 2), whereas group D pyroxenites are enriched in Cr (2200–15 000 ppm), with *cr*-number in the range 3–25 (Table 3; Fig. 4). Groups B and C are intermediate between these extremes (Cr = 850–4600 ppm; *cr*-number = 1–6). Altogether, the Ronda mafic rocks show a positive correlation between Cr and *mg*-number.

Similar to Cr, the other minor transition elements display large variations and, in some instances, are correlated with *mg*-number. Ni shows a positive correlation with *mg*-number, especially marked for group A, whereas Sc and V are negatively correlated with *mg*-number (Fig. 6). The lowest Ni (<300 ppm) and highest Sc and V concentrations (>40 and 250 ppm, respectively) occur in the most differentiated garnet granulites (*mg*-number < 65). Conversely, the highest Ni (>800 ppm) and lowest Sc and V concentrations (<20 and 100 ppm, respectively) are found in group D orthopyroxenites (*mg*-number > 85). Co, Cu and Zn contents are scattered when plotted vs *mg*-number, and their variations are unrelated to rock types. This dispersion may indicate that these elements are mainly hosted by sulphides.

Rare earth elements (REE)

The Ronda mafic rocks show a wide range of REE abundances (Table 3) and variable chondrite-normalized REE patterns (Fig. 7). The different rock types are generally characterized by distinct REE patterns. We distinguish four main types that roughly coincide with the four groups of mafic rocks.

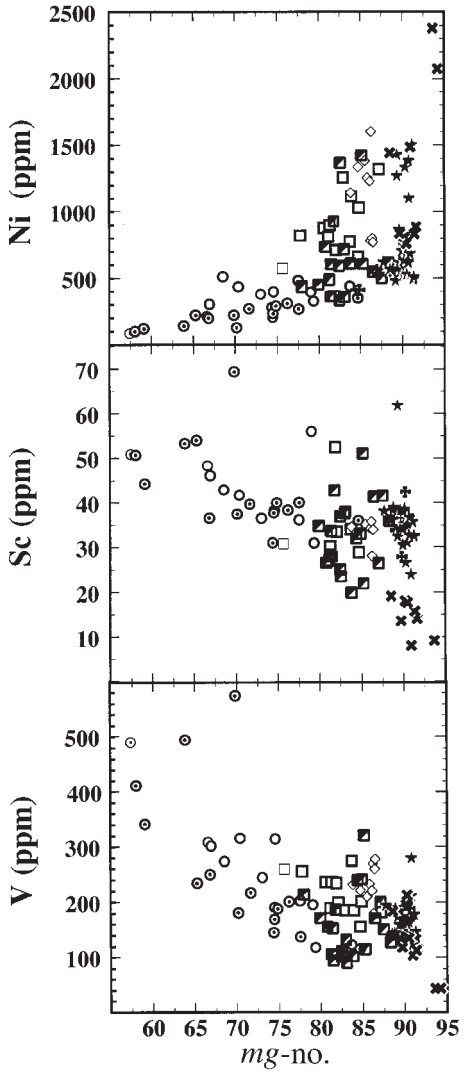

Fig. 6. Variation diagrams of Ni, Sc and V (ppm) vs *mg*-number for the Ronda mafic rocks. Symbols as in Fig. 4.

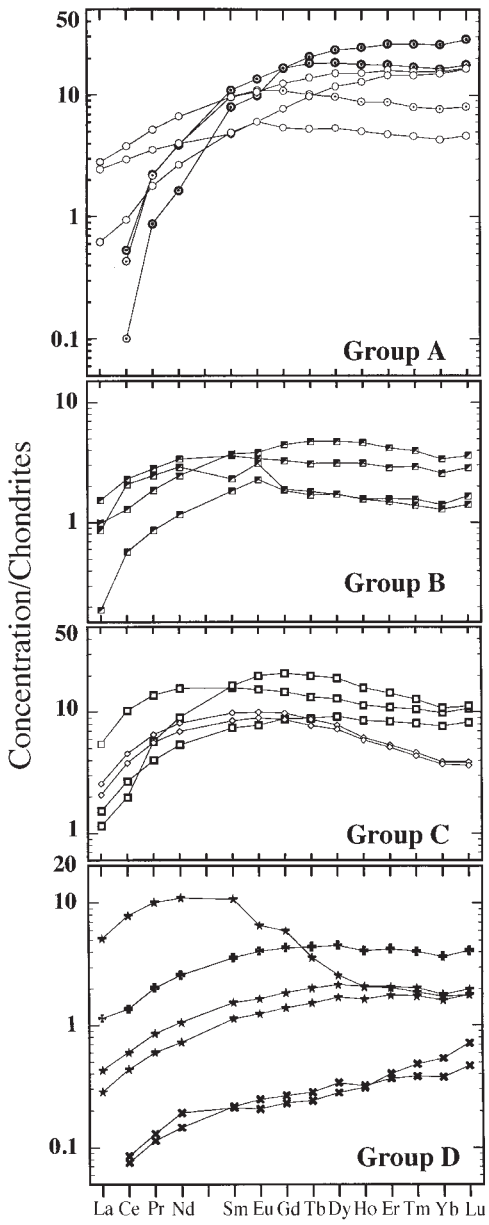

Fig. 7. Chondrite-normalized REE abundances in representative Ronda mafic rocks. Normalizing values after Sun & McDonough (1989). Symbols as in Fig. 4.

The type 1 REE pattern is strongly fractionated with high contents of heavy REE (HREE) (Yb_N = 8–35) (N indicates chondrite-normalized) and strongly depleted light REE (LREE) [Ce_N <1 and $(Ce/Yb)_N$ <0·05]. Middle REE (MREE)/HREE ratios are extremely variable [e.g. $(Gd/Yb)_N$ in the range 0·3–1·4]. This pattern is observed in most garnet mafic granulites (subgroup A1) and in several garnet pyroxenites (subgroup A2). Suen & Frey (1987) have already reported such REE patterns for Ronda mafic rocks.

The type 2 REE pattern resembles type 1 in being depleted in LREE relative to HREE. However, it is less fractionated [$(Ce/Yb)_N$ = 0·25–0·95], with HREE (Yb_N = 1·5–5) and LREE (Ce_N = 0·5–3) concentrations lower and higher, respectively, than in type 1 pattern (Fig. 7). This REE pattern is also distinguished by a slight, but distinct, positive anomaly of Eu (Fig. 7). The type 2 pattern is typical of group B mafic rocks (Fig. 7), where the highest HREE contents are found in samples with relics of garnet. It is also observed in two garnet pyroxenites (subgroup A2) with relatively high *mg*-numbers (79–84).

The type 3 REE pattern is convex-upward with depleted LREE and HREE relative to MREE. This pattern is characteristic of group C mafic rocks (Fig. 7). In detail, the REE patterns of subgroup C2 are 'bell-shaped' (Fig. 7), with a strong depletion of HREE relative to MREE [e.g. $(Gd/Yb)_N = 2{\cdot}25–2{\cdot}55$], whereas those of subgroup C1 are less convex and less depleted in HREE [$(Gd/Yb)_N = 0{\cdot}95–2{\cdot}0$]. Despite the high plagioclase content of some samples, group C mafic rocks do not show positive Eu anomalies, which confirms the subsolidus origin of plagioclase.

The type 4 REE pattern, typical of group D, is characterized by very low HREE content ($Yb_N = 0{\cdot}25–4$). In subgroup D1, where the modal proportion of clinopyroxene is high, such low HREE abundance is remarkable. Otherwise, these REE patterns are extremely variable in shape (Fig. 7) and show a wide range of $(Ce/Yb)_N$ values (0·1–5·3). Non-intrusive clinopyroxenites and websterites are depleted in LREE relative to HREE. Some of the samples with the lowest HREE content are selectively enriched either in LREE relative to MREE, with 'spoon-shaped' REE patterns [$(La/Nd)_N > 1$ and $(La/Yb)_N < 1$] (not shown in Fig. 7) or in LREE and MREE relative to HREE, with convex-upward REE patterns [$(La/Nd)_N < 1$ and $(La/Yb)_N > 1$]. The latter REE pattern is typical of group D intrusive dykes, which have $(Ce/Yb)_N$ around five compared with 0·1–1·1 in the rest of group D pyroxenites. The orthopyroxenites (subgroup D3) have the lowest REE abundances among the studied samples, with a steady decrease from HREE ($Yb_N = 0{\cdot}25–2$) to LREE ($Ce_N = 0{\cdot}025–0{\cdot}35$).

Other trace elements

Large ion lithophile elements (LILE; Rb, Ba, Sr, Th, and U)

Rb and Ba show a large variation, a weak positive correlation with each other, but no significant correlation with other incompatible elements. The highest Rb concentrations (1–4 ppm) are observed in samples from subgroup A1, C1 and group D intrusive dykes (Fig. 8). Lower Rb concentrations are found in most of group D samples (non-intrusive dykes) (0·1–1 ppm), and in some subgroup C2 and C1 samples (Fig. 8). Subgroup A2 and group B samples have intermediate concentrations (0·5–2 ppm). Ba concentrations are unrelated to rock types.

Sr is not correlated with other incompatible elements when the whole dataset is considered. Group A displays a broad negative correlation between Rb/Sr and *mg*-number. Also, a broad correlation is observed between Sr_N/Sr^* and Eu_N/Eu^* ($Sr^* = [(Pr_N + Nd_N)/2]$; $Eu^* = [(Sm_N + Gd_N)/2]$; N indicates primitive-mantle normalized). Moreover, Sr_N/Sr^* and Eu_N/Eu^* vary according to rock types:

(a) Most of subgroup A2, group C and D non-intrusive mafic rocks have Sr_N/Sr^* and Eu_N/Eu^* close to unity. These samples do not show—or show very subtle—Sr and Eu anomalies on primitive-mantle normalized diagrams (Fig. 8). In these rocks, Sr is relatively well correlated with LREE.

(b) Intrusive dykes have Sr_N/Sr^* and Eu_N/Eu^* values <1. These samples are distinguished by negative anomalies of Sr and Eu (Fig. 8). This feature suggests that plagioclase was involved in the evolution of their parental melts.

(c) HREE-enriched garnet granulites ($Yb_N > 10$) are distinguished from all the other samples by Sr_N/Sr^* values >1, whereas Eu_N/Eu^* is <1. Some group C rocks have subtle negative Sr anomalies, but no significant Eu anomalies. This observation indicates that a process other than plagioclase segregation was involved in the fractionation of Sr from LREE.

Th and U are positively correlated with each other and, to some degree, with LREE. Th/U and Th–U/LREE ratios display significant variations according to rock types. In particular, the majority of non-intrusive group D pyroxenites have $(Th/U)_N > 1$ (~1–3) whereas group D intrusive dykes and group C rocks have $(Th/U)_N < 1$. The Th/La ratio discriminates group D [$(Th/La)_N > 0{\cdot}25$] from group C [$(Th/La)_N < 0{\cdot}25$]. Groups A and B have extremely variable $(Th/U)_N$ and $(Th/La)_N$ ratios that encompass the range observed in group C and D.

Previous geochemical studies of Ronda mafic layers have suggested that their contents in Rb, Sr, and possibly other LILE, were strongly affected by secondary alteration processes (Polvé & Allègre, 1980; Zindler *et al.*, 1983), yet these elements show several features suggesting that their distribution is, overall, mostly governed by mantle processes. These features include correlations between Rb and rock types, between Rb/Sr and *mg*-number in group A, and between Sr and Eu—or LREE—in several samples. In fact, recent Nd–Sr isotopic data on acid-leached cpx from the Beni Bousera massif (Northern Morocco) support contamination by a crustal component, but indicate that this component was very probably introduced in mantle conditions (J. Kornprobst, personal communication, 1998). Moreover, ICP-MS data on separated and leached minerals from Ronda samples indicate that Rb, Sr and other LILE are essentially hosted by minerals and/or mantle-derived fluid inclusions (Bodinier *et al.*, 1996; Garrido & Bodinier, 1998).

High field strength elements (HFSE; Nb, Ta, Zr, and Hf)

Nb and Ta are broadly correlated with each other and with LREE, but with significant Nb/Ta and Nb–Ta/LREE variations according to rock types. Subgroup D2 and most group B samples are characterized by relatively

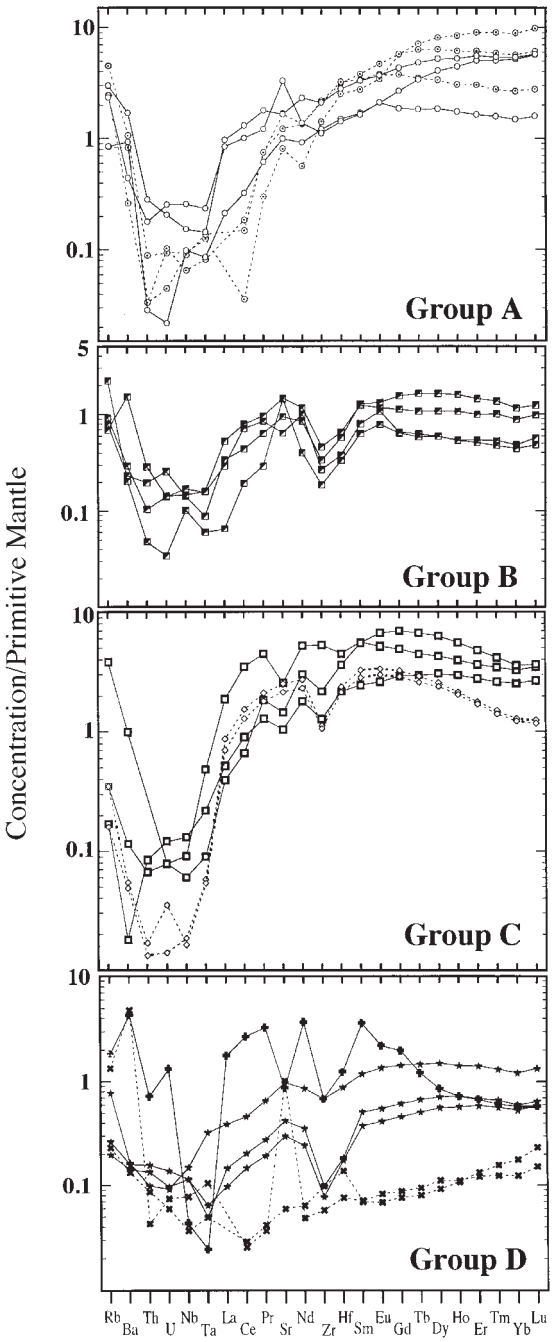

Fig. 8. Primitive mantle-normalized trace element abundances in representative mafic rocks of the Ronda massif. Trace elements are arranged according to the presumed order of decreasing incompatibility (from Rb to Lu) in the basalt–peridotite system (Sun *et al.*, 1979). Normalizing values after Sun & McDonough (1989). Symbols as in Fig. 4 [except +, intrusive dyke (Group D)].

high $(Nb/Ta)_N$ ratios (0·9–2·5), whereas group C is distinguished by low $(Nb/Ta)_N$ (0·2–0·6). Groups A and subgroups D1 and D3 have intermediate $(Nb/Ta)_N$ (0·5–1). The Nb–Ta/LREE ratios are negatively correlated with LREE abundances. The intrusive dykes show the lowest Nb–Ta/LREE ratios. Conversely, subgroup D3 is distinguished by relatively high Nb–Ta/LREE values coupled with low LREE abundances.

Zr and Hf are strongly correlated with each other and MREE. The Zr/Hf ratio is systematically lower than primitive mantle values [$(Zr/Hf)_N$ = 0·4–0·9], without significant variations according to rock types. The different groups are well discriminated by Zr_N/Zr^* [$Zr^* = (2 \times Nd_N + Sm_N)/3$]. Most of the samples show a positive correlation between Zr_N/Zr^* and MREE, from Zr_N/Zr^* ~0·1 in the most MREE-depleted samples (non-intrusive subgroup D1) up to values close to unity in the most MREE-enriched samples (group A and several samples of group C). In other words, the normalized patterns of groups A, B, C and non-intrusive D1 and D2 pyroxenites show a negative anomaly of Zr (±Hf), which is only very subtle in the MREE-enriched samples (groups A and C), whereas it is well marked in the MREE-poor samples (groups B and D) (Fig. 8). Two exceptions are the orthopyroxenites (subgroup D3), which have Zr_N/Zr^* close to unity despite their very low MREE content, and the intrusive dykes, which have low Zr_N/Zr^* ratios despite their high MREE content (Fig. 8).

DISCUSSION

Analogies with other mantle mafic rocks and melts, and primary mineralogy of Ronda mafic rocks

It has been demonstrated that the whole-rock compositions of mafic layers and veins in Ronda and other lherzolite massifs are not similar to those of known erupted magmas (Frey *et al.*, 1985; Bodinier *et al.*, 1987*b*; Suen & Frey, 1987), yet there is a general consensus that these rocks originated via open-system, magmatic processes. Like equivalent rock types from mantle xenoliths (Irving, 1980), they are generally interpreted as high-pressure cumulates and considered to represent mineral segregates in magma conduits. However, their 'primary' mineralogy may be modified by later magmatic processes such as partial melting and metasomatism, and may therefore evolve through successive open-system stages. Even when it has been obscured by metamorphic recrystallization, the primary mineralogy associated with the last magmatic stages can be constrained by major and trace element data, as discussed below.

Group A

Most of group A samples show strongly fractionated REE patterns similar to those of garnet pyroxenites from Beni

Bousera (Pearson *et al.*, 1991, 1993) and the Pyrenean lherzolite massifs (Bodinier *et al.*, 1987*b*) (Fig. 9a). In the Pyrenees, these REE patterns are observed in pyroxenites containing relics of magmatic garnet (Bodinier *et al.*, 1987*b*). Two subgroup A2 samples display REE normalized patterns with flat MREE–HREE segments and slight, positive Eu anomalies (type 2 REE patterns), which may reflect the presence of primary plagioclase. These REE patterns resemble those of corundum-bearing garnet pyroxenites with positive Eu anomalies from the Beni Bousera massif (Northern Morocco) (Fig. 9a; Kornprobst *et al.*, 1990; Pearson *et al.*, 1993). In Beni Bousera, these pyroxenites have been interpreted as recycled oceanic gabbros recrystallized at high-pressure mantle conditions (Kornprobst *et al.*, 1990). From their low *mg*-number, their silica oversaturation and the occurrence of Eu anomalies in some samples, group A1 mafic layers and equivalent rock types from Beni Bousera are clearly distinguished from garnet-bearing mafic rocks in other orogenic peridotites.

The following observations indicate that the primary magmatic assemblage of group A was dominated by clinopyroxene and garnet: (a) whole-rock compositions plot on, or to the right of (i.e. above), the pyroxene–garnet plane in the CMAS projection of Fig. 10a; (b) they have high Al_2O_3 contents; (c) they show high contents of trace elements compatible in garnet, such as HREE and Sc (Figs 5 and 6); (d) their chondrite-normalized REE patterns are strongly fractionated. The fact that group A mafic rocks are aligned along the clinopyroxene projection in the FeO vs MgO diagram (Fig. 10c) indicates that this mineral was the predominant primary phase.

The silica oversaturation of most subgroup A1 samples (Fig. 10a) implies the presence of a primary silica-saturated mineral (e.g. quartz or/and plagioclase). As the normalized REE patterns of subgroup A1 do not show a Eu anomaly (Fig. 7), primary plagioclase is unlikely. On the other hand, relics of quartz have been found in some samples (Obata, 1980). This mineral might have

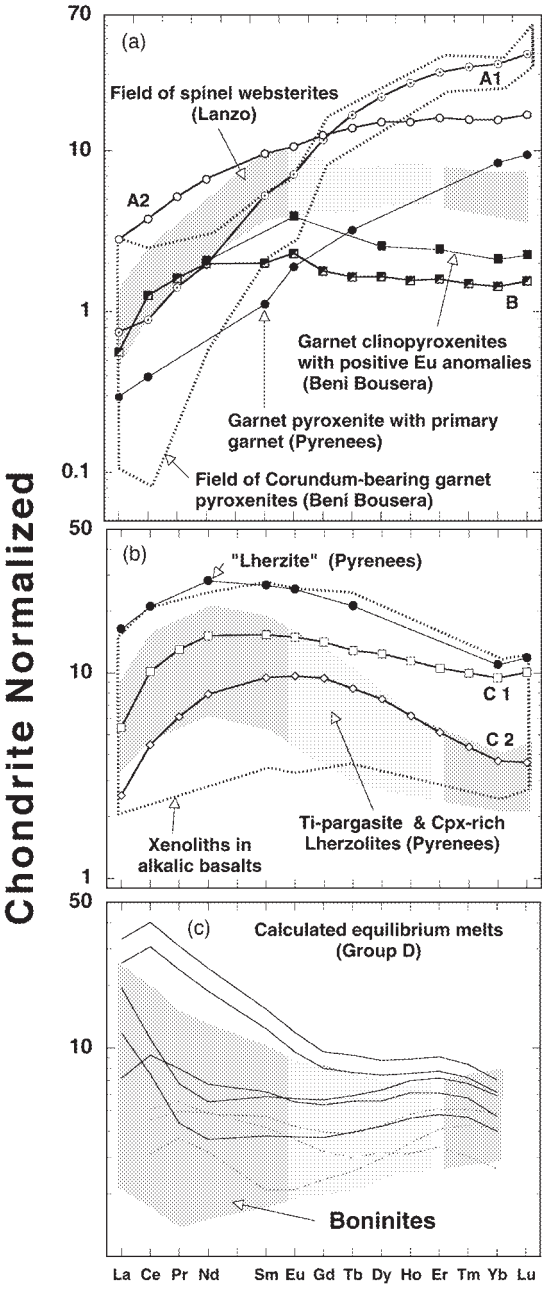

Fig. 9. (a and b) Chondrite-normalized REE diagrams comparing representative samples of groups A, B and C mafic rocks from Ronda with mafic rocks from other orogenic peridotites and mantle xenoliths. Symbols as in Fig. 4. Normalizing values after Sun & McDonough (1989). Data sources: corundum-bearing garnet pyroxenites from Beni Bousera (Northern Morocco) after Pearson *et al.* (1993); garnet pyroxenites from Beni Bousera with a positive Eu anomaly after Kornprobst *et al.* (1990)—these rocks have been interpreted as oceanic gabbros recycled into the mantle; garnet pyroxenites with primary magmatic garnet from the Lherz massif (Pyrenees, Southern France) after Bodinier *et al.* (1987*b*); spinel websterites from Lanzo (Northern Italy) after Bodinier (1989); Ti-pargasite and clinopyroxene-rich lherzolites from the Caussou massif (Pyrenees, Southern France) after Fabriès *et al.* (1989); lherzite (= hornblendite veins) from the Lherz massif after Bodinier *et al.* (1987*b*); mantle xenoliths from continental alkaline basalts after Irving (1980). (c) Selected chondrite-normalized REE composition of melts in equilibrium with group D mafic rocks (continuous lines, subgroup D1; dashed lines, subgroup D3). The modal compositions are estimated by mass balance using the whole-rock major composition and mineral composition of mafic rocks. Equilibrium melts are then computed using these modes, the REE whole-rock composition of mafic rocks, and experimental mineral–melt partition coefficients [cpx–melt after Hart & Dunn (1993); opx–melt and ol–melt after Kelemen *et al.* (1993)]. Where it was not available (e.g. Pr), the partition coefficient was interpolated between coefficients of elements with similar compatibility. The dark field is the chondrite-normalized REE compositional field of boninites using data of Hickey & Frey (1982), Cameron *et al.* (1983) and Cameron (1989).

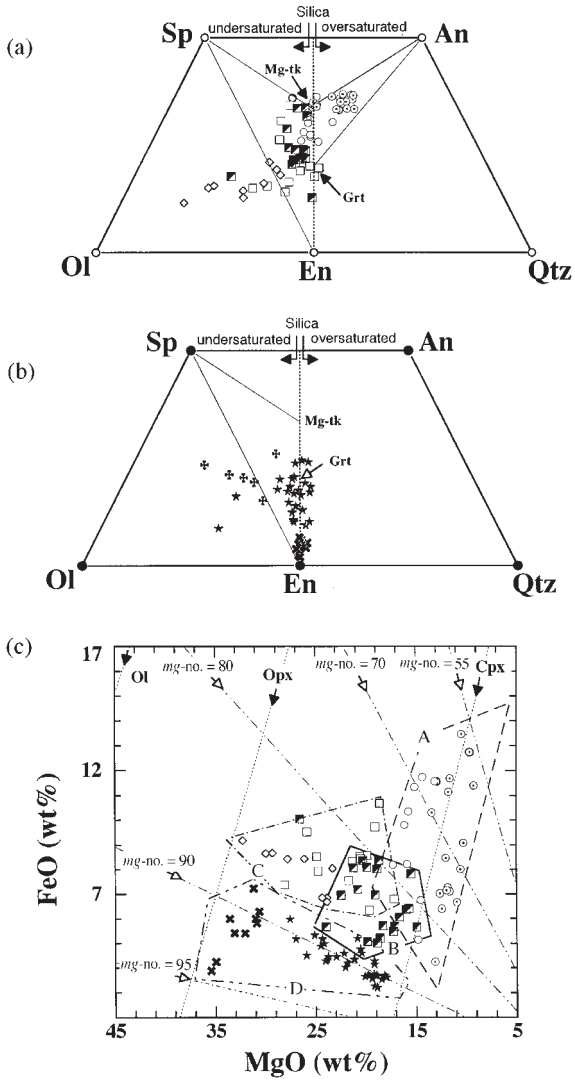

Fig. 10. (a and b) Ol–Sp–An–Qtz quadrilaterals showing the projected compositions of Ronda mafic rocks into the plane defined by the poles Catk (Ca-Tschermak), Ol (olivine) and Qtz (quartz), in the condensed CaO–MgO–Al_2O_3–SiO_2 (CMAS) system (oxide mol %). Diopside is used as projection point (the Catk apex is not shown in the figure). The dotted line in the middle of the quadrilateral is the projection of the pyroxene–garnet plane (i.e. the silica saturation plane, in a normative sense, at high pressure). This line divides the quadrilateral into two parts: a silica-undersaturated domain to the left (i.e. below the pyroxene plane in the CMAS system) and a silica-oversaturated domain to the right (i.e. above the pyroxene plane in the CMAS system). The end-member components condensed into the phase poles are as follows: Olivine (Ol: forsterite, fayalite); Spinel (Sp: spinel, hercynite, chromite); Ca-Tschermak (Catk; catk, jadeite, kosmochlore); Plagioclase (An: anorthite, albite); Garnet (Grt: almandine, pyrope); Diopside (Di: diopside, hedenbergite); Enstatite (En: enstatite, ferrosillite). (c) MgO vs FeO (wt %) variation diagram for the Ronda mafic rocks. Symbols as in Fig. 4. Also projected are the *mg*-number isolines for several *mg*-number values (dashed–dotted lines), and the projections onto the MgO–FeO plane of the binary solid-solution of clinopyroxene (Cpx: diopside–hedenbergite), orthopyroxene (Opx: enstatite–ferrosillite) and olivine (Ol: forsterite, fayalite) (dotted lines).

been almost entirely consumed during the late eclogite-to-garnet granulite metamorphic reactions that are characteristic of this subgroup (Garrido, 1995). Alternatively, the silica excess may be explained by solid-solution of a non-stoichiometric (silica-oversaturated) component in the primary clinopyroxene (e.g. 'eskola' component).

Group B

The REE normalized patterns of some group B samples resemble those of Beni Bousera garnet pyroxenites with positive Eu anomalies (Fig. 9a). However, group B pyroxenites differ from the Beni Bousera samples by higher *mg*-number and lower Na_2O, Al_2O_3 and CaO contents (Fig. 5). From their major element composition, group B pyroxenites are more comparable with the spinel websterites from Lanzo and Pyrenees (Figs 5 and 9a), but they are distinguished by lower REE abundances.

Group B chemical compositions are consistent with variable proportions of primary clinopyroxene, orthopyroxene, spinel, plagioclase and, in some samples, olivine. This primary mineralogy is similar to their current mineralogical composition. The presence of primary spinel is suggested by the high Al_2O_3 content (Fig. 5) and silica undersaturation (Fig. 10b). Also, high MgO, Ni and Co contents (Fig. 6) are indicative of primary orthopyroxene and, in some samples, olivine. Furthermore, the slight positive Eu anomalies in most samples implies the presence of primary plagioclase. This mineral occurs in disequilibrium assemblages that resulted from breakdown of garnet in open system at relatively low pressure (~1·2 GPa). This interpretation is supported by the fact that group B samples with the higher HREE abundances (Fig. 7b) still preserve textural evidence of garnet (Fig. 3c). The samples devoid of garnet relics have lower HREE abundances and more marked positive Eu anomalies.

Group C

Convex-upward REE patterns similar to those of group C have been reported in pyroxenite xenoliths interpreted as magmatic segregates crystallized from LREE-enriched alkaline melts (Frey, 1980; Irving, 1980) (Fig. 9b). Similar REE patterns are also observed in alkaline pyroxenite dykes and their wall rocks in Pyrenean peridotites (Bodinier *et al.*, 1987*a*, 1990) (Fig. 9b). The 'bell-shaped' REE patterns of subgroup C2 are especially similar to those observed in clinopyroxene-rich peridotites from Caussou (Pyrenees; Fig. 9b), which have been ascribed to clinopyroxene-forming reactions between alkaline melts and spinel peridotites (Bodinier *et al.*, 1988; Fabriès *et al.*, 1989; Downes *et al.*, 1991).

We distinguish three primary magmatic assemblages in this group. The first is composed of clinopyroxene and orthopyroxene, and corresponds to most of subgroup C1 samples. These rocks plot on the pyroxene–garnet

plane of Fig. 10a, and between the orthopyroxene and clinopyroxene projections of Fig. 10c. The presence of primary orthopyroxene is sustained by their relatively low CaO contents compared with group A (Fig. 5). The second primary assemblage is composed of orthopyroxene, clinopyroxene and spinel, and corresponds to the rest of subgroup C1. In Fig. 10a, these samples plot well to the left of the pyroxene–garnet plane (i.e. silica undersaturated), within the Sp–En–Mgtk triangle. The third assemblage corresponds to subgroup C2 and is composed of orthopyroxene, olivine, clinopyroxene and spinel. These samples plot towards the olivine projection in Fig. 10c, and within the Sp–En–Ol triangle in Fig. 10a. Finally, the relatively low Al_2O_3, V, Sc and HREE contents (Figs 5–7), and the fact that, for a similar Al_2O_3 content, this group has lower SiO_2/MgO ratio than group A, indicate that garnet was not a magmatic phase in group C mafic rocks.

Group D

The REE patterns of theoretical melts in equilibrium with subgroups D1 (except for intrusive dykes) and D3 mafic rocks are characterized by low HREE abundances (Fig. 9c). These REE patterns are comparable with those of boninites found in subduction settings (Fig. 9c) [Crawford (1989) and references therein]. The boninite-like geochemical signature of group D samples is also consistent with their elevated *mg*-number, Cr and Ni abundances, and low *ti*-number. Mafic rocks with such low HREE abundances have been described from the mantle section of some ophiolites (Varfalvy *et al.*, 1996).

Melts in equilibrium with intrusive dykes are very similar to high-*mg*-number andesites with respect to trace elements (Fig. 11). The LILE-enriched, HFSE-depleted pattern of these rocks cannot be solely explained by their modal composition. To our knowledge, this trace-element signature has never been reported from orogenic peridotites. On the other hand, it has been observed in calc-alkaline suites such as high-*mg*-number andesites (e.g. Rogers & Saunders, 1989; Kelemen, 1995) and lower continental crust granulites (e.g. Mattie *et al.*, 1997) (Fig. 11). This geochemical signature is rather similar to that postulated for the average continental crust (e.g. Rudnick & Fountain, 1995). It is also commonly found in mantle xenoliths of lithospheric peridotites metasomatized by LILE-enriched mantle melts (Hauri *et al.*, 1993; Rudnick *et al.*, 1993; Bedini *et al.*, 1997). Owing to the presence of intrusive dykes with this geochemical affinity, Ronda differs from other subcontinental orogenic massifs such as Lherz, where intrusive dykes have an alkaline signature (Bodinier *et al.*, 1987*a*). In this respect, Ronda is more comparable with the mantle section of back-arc ophiolites and arc complexes, where intrusive dykes and websterites have a calc-alkaline signature (e.g. Kelemen & Dick, 1995).

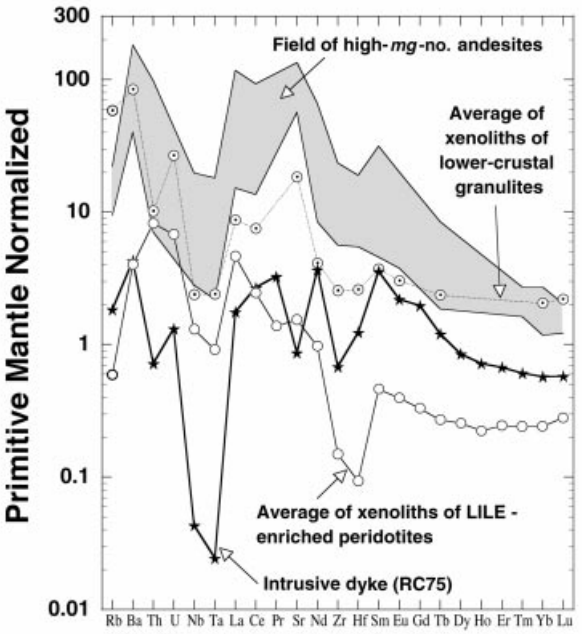

Fig. 11. Primitive mantle-normalized diagram comparing the trace element composition of a group D intrusive websterite from Ronda with other LILE-enriched, HFSE-depleted rock types of mantle origin: high-*mg*-number andesites from Mexico (Rogers & Saunders, 1989), lower-crust xenoliths from the western USA [average of three samples reported by Mattie *et al.* (1997)], and LILE-enriched mantle xenoliths from the East African Rift [average of the deformed, apatite-bearing xenoliths of Bedini *et al.* (1997)]. Normalizing values and trace element arrangement after Sun & McDonough (1989).

Whole-rock compositions of group D can be explained by variable proportions of orthopyroxene, clinopyroxene, olivine and subordinate amount of spinel. Such primary assemblage is similar to the current mineralogy of the samples, but modal proportions were modified by exsolution processes. In Fig. 10b, the samples plot between opx and cpx projections. The orthopyroxenites (D3) and the clinopyroxenites (D1) project towards the corresponding end-members, whereas the websterites plot between them. Modal variations of primary orthopyroxene, clinopyroxene and olivine may account for the dispersion of SiO_2, CaO, Ni and Sc contents in this group (Figs 5 and 6). The high Zr–Hf/MREE values typical of the orthopyroxenites may be explained by preferential partitioning of these elements in orthopyroxene (Rampone *et al.*, 1991), confirming that this mineral crystallized in open system. Group D mafic rocks plot at high, and relatively constant, *mg*-number values (Figs 4 and 5) comparable with the peridotite values (~90). This indicates that changes in the solidus mineralogy took place without significant changes in the *mg*-number of the melt, a feature that is characteristic of melts that evolve via a melt–peridotite reaction process (Kelemen, 1986, 1990).

Relative age constraints on the individualization and chemical differentiation of mafic rocks

The sequence of structural events is well established in the Ronda peridotite (Van der Wal & Bodinier, 1996; Van der Wal & Vissers, 1996). Combination of structural observations and geochemical data of mafic rocks allows us to compare the timing of their formation with the structural events recognized in the host peridotites.

Group A mafic rocks have been deformed by the tectonic event that originated the spinel tectonite domain (Figs 2a, 3a and b). This observation implies that the layers are older than this tectonic event. Limited Re–Os isotopic data for four group A samples (Reisberg *et al.*, 1991; L. Reisberg personal communication, 1998) indicate model ages around 1–2 Ga. This clearly shows that these mafic layers are old features, isolated in the lithospheric mantle a long time ago. On the other hand, the Nd systematics of one sample of likely group A affinity (Zindler *et al.*, 1983) shows that its whole-rock $^{143}Nd/^{144}Nd$ is MORB like although its Sm/Nd ratio is extremely high. This may suggest that LREE contents and/or Nd isotopes of group A were cryptically modified during the magmatic event that formed the recrystallization front. In fact, the positive correlation of Ce vs *mg*-number may result from re-equilibration of low-*mg*-number, group A pyroxenites with small fractions of LREE-enriched melts infiltrated in the spinel tectonite domain during this event. Such a process was envisaged by Van der Wal & Bodinier (1996) to explain the distribution of LREE and other highly incompatible elements in the spinel tectonites. More isotopic work on group A layers with variable *mg*-number and Ce/Sm values is needed to evaluate the extent to which the mafic rocks have been affected by cryptic metasomatism.

Group B mafic rocks display field structures comparable with those of group A. However, group B usually shows coarse-grained microstructures without plastic deformation fabrics, except perhaps for an inherited LPO in pyroxenes. These observations, as well as the presence of relics of garnet, indicate that group B derives from the recrystallization of former group A, garnet-bearing protoliths. Group B is therefore younger than group A. However, closed-system recrystallization at the expense of group A cannot account for the chemistry of group B. Group A and B mafic rocks have distinct primary assemblages and trace-element compositions implying that group B was formed in open system, by magmatic replacement of group A. As group B layers are spatially confined to the coarse-grained granular subdomain (Fig. 1), this process was probably related to the porous flow event inferred for the development of the recrystallization front (Van der Wal & Bodinier, 1996).

Relative age constraints on group C mafic rocks are precluded by the lack of cross-cutting relationships of these layers with the spinel tectonite structures and/or other mafic layers. However, several field observations indicate that this group was formed after the development of the spinel tectonite domain and somewhat after the recrystallization front. First, in contrast to groups A and B, group C does not display the highly deformed field structures typical of the spinel tectonite domain, but occurs as almost undeformed 'sill-complexes' (Fig. 3b). Second, mafic rocks with group C chemistry occur only well behind the recrystallization front (i.e. at >1 km to the SE: Fig. 1), closely associated with harzburgites and dunites of the layered-granular subdomain, as well as with similar harzburgite–dunite sequences in the plagioclase tectonite domain. Field and petrographic observations indicate that the refractory layers (harzburgites and dunites) overprint the coarse-granular subdomain associated with the recrystallization front and represent the last regions where porous flow was eventually focused in the massif (Remaïdi, 1993; Van der Wal & Bodinier, 1996). Group C must be somehow related to this magmatic stage. However, group C pyroxenites are strongly affected—at least locally—by the olivine-forming reactions that have generated the refractory peridotites (harzburgites and dunites). This implies that the pyroxenites are somewhat older that the refractory peridotites (Remaïdi, 1993). These observations constrain the formation of group C between the development of the recrystallization front and that of refractory layers in the granular peridotite and plagioclase tectonite domains.

Field and microstructural observations indicate that concordant group D mafic layers are younger than group A and B layers. In the field, group D layers display the same deformation structures as the mafic layers of the spinel tectonite domain but show undeformed, coarse-grained textures (Fig. 3e). This feature is ascribed to coeval recrystallization and magmatic replacement of previous group A and B mafic rocks, as demonstrated by the composite layers. Concordant group D mafic rocks mostly occur throughout the granular domain and in composite layers on both sides of the recrystallization front (Fig. 1). Hence, this facies is clearly younger than the recrystallization front. Group D locally replaces group C pyroxenites, but the replacement is incipient compared with that observed in group A and B layers. Only locally, within the refractory peridotites of the layered-granular subdomain, is the replacement nearly complete. Overall, field relationships indicate that the development of groups C and D largely overlapped in time, but group D was somewhat later. The existence of intrusive group D dykes (Fig. 2f) confirms that group D records a very late magmatic stage in Ronda.

On the basis of these observations, we conclude that the generation and chemical differentiation of Ronda mafic layers took place during at least two separate mantle events. Group A mafic layers are old. Their formation is unrelated

to the present petrological zoning of Ronda peridotites and occurred before the development of the spinel tectonite domain. Group B, C and D mafic rocks are related to different stages of the magmatic event that led to the development of the recrystallization front and the granular domain. Therefore, their geochemical differentiation is intimately associated with the development of the present tectonic and petrologic zoning of the massif. In addition, the diversity of groups B, C and D reflects significant variations in the petrogenetic processes involved in their formation. Groups B and D layers have replaced former mafic layers (B replaced A and D replaced A, B or C), group C layers have replaced peridotites, and group D dykes are mineral segregates in open melt conduits.

Origin of the petrological and chemical zoning of Ronda mafic rocks

Our results indicate that major textural, mineralogical and chemical changes in Ronda mafic rocks occur in the transition between the structural, petrological and geochemical domains identified in the peridotites (Obata, 1980; Van der Wal & Bodinier, 1996; Van der Wal & Vissers, 1996). In particular, the transition from group A to group B at the recrystallization front represents not only distinct textural and mineralogical changes in the mafic layers, but also a major discontinuity in their chemical composition. This observation indicates that the magmatic process responsible for the transition of group A to group B mafic layers was coeval with the magmatic event inferred for the development of the recrystallization front and the granular peridotite domain (Van der Wal & Bodinier, 1996).

The model that emerges from our data differs from the one proposed in previous studies. Suen & Frey (1987) hypothesized that the Ronda mafic layers were related to a single magmatic event whereby mineral segregates formed on the walls of magma conduits in a mantle diapir; however, they admitted several complexities in their data that could not be explained by a single stage model. For example, a single magmatic event does not account for the relative LREE depletion of the most differentiated mafic rocks (group A) compared with more primitive members (group C) (Fig. 7), nor for the existence of two distinct geochemical trends in the Ti–*mg*-number variation diagram (Fig. 4). Our study establishes a temporal sequence for the formation of mafic layers and demonstrates the importance of successive melt–rock reactions to account for their diversity.

Van der Wal & Bodinier (1996) proposed that the Ronda recrystallization front and granular peridotite domains were developed during a major heating and magmatic event that affected previously thinned subcontinental lithosphere. This event probably reflects thermal and compositional modification of thinned subcontinental lithospheric mantle by upwelling asthenosphere, related either to passive (Tubia & Cuevas, 1986; Tubia, 1994) or active (Platt & Vissers, 1989; Vissers *et al.*, 1995; Van der Wal & Vissers, 1996) tectonic extension of the lithosphere. During this event, a piece of thinned, veined lithospheric mantle, vestiges of which are now represented by the spinel tectonite domain in the Ronda massif, was partially melted and pervasively infiltrated by asthenospheric melts. The compositional and petrological diversity of Ronda mafic layers was shaped during this major geodynamic event. In this tectonic scenario, we discuss below the origin of groups B, C and D mafic layers as recording three distinct stages of thermal and magmatic 'erosion' of subcontinental lithosphere. The origin and chemical differentiation of group A mafic layers will be addressed in a forthcoming paper.

Group B: replacement of garnet-bearing mafic layers via melt-producing melt–rock reactions during the thermal climax of heating of the lithosphere

Group B mafic rocks were formed after former group A layers during the development of the granular peridotites. We interpret this stage as the thermal climax of erosion and melting of the thinned lithosphere. At this stage, the granular peridotites were partially melted in seiland subfacies *P–T* conditions (~1·3 GPa, Van der Wal & Vissers, 1993; and >1280°C, Remaïdi, 1993; see also Van der Wal & Bodinier, 1996). However, the composition of group B mafic layers cannot be explain by simple partial melting of group A mafic rocks. Compared with group A, group B is more enriched in LREE, has higher Ce/Sm ratios, and is depleted in Zr and Hf relative to MREE (Fig. 8). More likely, group B was formed by melt-producing reactions between group A layers and partial melts of the host peridotites that circulated pervasively by porous flow through the granular domain. This scenario requires that the reacting melts had higher LREE/HREE ratios than the protolith (i.e. group A layers). As group A is considerably depleted in LREE, with lower LREE/HREE ratio than the host spinel tectonite peridotites [see Frey *et al.* (1985) and Van der Wal & Bodinier (1996) for the REE content of the spinel tectonites], reaction of these layers with melts percolating through—and equilibrated with—the granular peridotites resulted in LREE enrichment in reacted rocks (groups B) compared with protoliths (group A).

Petrographic observations suggest the following melt–rock reaction: grt + Al-cpx (± pl) + melt1 = opx + sp (± pl) + melt2. At these *P–T* conditions, reaction of garnet-bearing mafic rocks with olivine-saturated melts occurred at increasing melt mass (melt1 < melt2), and produced reacted lithologies comparable with group B, garnet-free websterites. Group B garnet websterites are interpreted as transitional reactional assemblages.

We emphasize that negative anomalies of Zr and Hf characteristics of group B are seemingly a signature

inherited from the melt–rock reaction process, as predicted by Kelemen *et al.* (1989). This is suggested by the existence of a strong negative anomaly of Zr and Hf in Ronda refractory peridotites produced by melt–rock reaction (Remaïdi, 1993), as well as by the observation that the most reacted layers (i.e. group D; see below) show deeper negative anomalies of these elements than any other mafic rock in Ronda.

Group C: replacement of peridotites via near-solidus, melt-consuming reactions upon thermal relaxation of the lithosphere

As discussed above, this group was formed later than group B and somewhat earlier than—or contemporaneous with—group D pyroxenites. Therefore, group C records a magmatic stage that probably occurred right after the thermal climax responsible for the development of the recrystallization front and the granular peridotite domain.

In spite of its layered structure comparable with sill complexes, group C was formed by metasomatic replacement of peridotites, rather than by melt crystallization in magmatic sills. Field evidence for a metasomatic origin includes the presence of interlayered flames of host peridotites within thick websterite layers (Fig. 2b). This metasomatic origin can be accounted for by melt-consuming reaction at temperatures close to the anhydrous peridotite solidus, upon cooling of the porous flow domain responsible for the recrystallization front. During this stage, interstitial melt became saturated in pyroxene ($\pm$ aluminous phases) and reacted with olivine from the host peridotites producing clinopyroxene, orthopyroxene and spinel ($\pm$ amphibole, upon further cooling). Depending on the melt/rock ratio (i.e. pervasive or channelled porous flow), the reaction resulted either in diffuse 'fertilization' of the peridotites (i.e. producing secondary lherzolites) or in the formation of websterite sequences. In Ronda, the first situation is represented by the 'secondary' lherzolites typical of the fine-granular subdomain (Van der Wal & Bodinier, 1996), whereas the second corresponds to group C layers. Websterites with olivine-rich relics of the host peridotites (group C2) record transitional reactional stages at moderate melt/rock ratio, whereas olivine-free websterites (group C1) represent the final reaction products at high melt/rock ratio.

Reisberg *et al.* (1991) studied the Re–Os systematics of two samples of type C affinity from the eastern part of the massif (L. Reisberg, personal communication, 1998). The $^{187}Os/^{186}Os$ ratios of these samples are lower than those of group A samples, but still distinctly higher than typical mantle values. Reisberg *et al.* found ancient model ages for these samples. At first sight, these results are in conflict with our field observations indicating that group C layers were individualized during a late evolutionary stage of Ronda. In fact, isotopic and field data may be reconciled by considering that the percolating melts responsible for the individualization of group C layers involved two distinct components: (1) an alkaline melt infiltrated from a deep-seated, asthenospheric source—this component is suggested by the convex-upward REE patterns typical of this group (Fig. 9a); (2) partial melts from old, veined lithospheric mantle similar to that exposed in the spinel tectonite domain. A significant contribution of the strongly radiogenic garnet pyroxenites (group A) to the 'lithospheric' melt component would account for relatively high $^{187}Os/^{186}Os$ ratios of group C. Such explanation is consistent with the scenario envisioned here for the late evolution of Ronda massif. If confirmed by further isotopic data, it would indicate that lithospheric mafic rocks may significantly contribute to partial melts produced during heating and melting of mantle lithosphere.

The strong melt localization and high melt/rock ratio implied by the formation of group C layers may be accounted for by 'refraction' and channelling of percolating melts below the freezing horizon represented by the base of the thermal lithosphere (Sparks & Parmentier, 1991; Spiegelman, 1993; Xu *et al.*, 1998). The suite of group C layers found in the granular peridotite and plagioclase tectonite domains is thought to record the retrograde evolution of the peridotite solidus isotherm, during the thermal relaxation that followed the development of the recrystallization front. The websterite layers would represent successive positions of the solidus isotherm—and hence of the permeability boundary of the basaltic porous flow domain—while the latter was receding down to gradually deeper mantle levels. A similar melt–rock reaction origin was recently proposed for thick (>10 m) websterite layers in the base of the obducted Kohistan arc (Jijal complex, Northern Pakistan) (Burg *et al.*, 1998). The Jijal complex illustrates a scenario whereby the websterite-forming, melt-consuming reaction occurred during cooling associated with lithospheric thickening beneath an active island arc. Ronda represents a situation where the reaction was associated with thermal relaxation of thinned subcontinental lithosphere.

Group D: metasomatic replacement of mafic layers via melt–rock reactions involving small fractions of Mg-rich, calc-alkaline melts during the waning stages of melt porous flow activity

Concordant group D pyroxenites were formed by metasomatic replacement of previous mafic layers by melts percolating pervasively through the host peridotites. The fact that this group overprints group C pyroxenites, as well as the existence of group D cross-cutting dykes, indicates that group D records a magmatic event that

probably lasted until early emplacement of the massif into the crust. We think that group D mafic rocks resulted from pervasive percolation of volatile-rich small melt fractions that were residual after olivine- and melt-consuming reactions such as those invoked for the development of group C mafic layers. These small melt fractions were highly mobile and migrated throughout the Ronda massif until late cooling stages, down to lithospheric temperatures. Therefore, group D layers—and composite layers—would record the waning stages of melt porous flow.

Several observations support the hypothesis that group D records the evolution of volatile-rich small melt fractions until the last stages of melt percolation activity. First, field evidence indicates that the percolation event responsible for their development was active at least until the temperatures recorded by harzburgite–dunite sequences in the granular peridotite and plagioclase tectonite domains. These refractory peridotites are spatially associated with group D layers in these domains, where they clearly overprint group C layers (Gervilla & Remaïdi, 1993). Therefore, they are late magmatic features in the mantle history of Ronda (Remaïdi, 1993). These harzburgite–dunite sequences typically yield low temperatures (1160°C) that are thought to record the recess of melt porous flow activity (Remaïdi, 1993). Furthermore, the presence of amphibole-bearing peridotites in these sequences provides evidence for the circulation of water-rich melts down to temperatures of ~1060°C (Remaïdi, 1993). Second, the pervasive character of the percolation event recorded by the parental melts of group D is demonstrated by the fact that they invaded lithospheric peridotites beyond the thermal 'permeability barrier' for basaltic melts represented by the recrystallization front (Van der Wal & Bodinier, 1996). At first sight, this pervasive process may be in conflict with the idea of progressive receding and channelling of melt porous flow upon thermal relaxation of the massif proposed to account for the formation of group C layers. However, the two processes may be reconciled by assuming that two distinct magmatic percolation systems existed at this stage in Ronda. One system was responsible for the recrystallization front, the granular domain (including the harzburgite–dunite sequences) and the related group B and C pyroxenite layers. This porous flow system was associated with high fractions of basaltic melts that were gradually channelled upon receding of the percolation domain. The other percolation system, responsible for the development of group D pyroxenites, was associated with residual volatile-rich melts produced after melt-consuming reactions. Because of their low viscosity and solidification temperature, such melts are able to migrate as small fractions and pervasively infiltrate large volumes of relatively cold, lithospheric peridotites (Watson & Brenan, 1987; McKenzie, 1989). Hence, these small melt fractions were able to percolate beyond the recrystallization front in regions where basaltic porous flow receded upon cooling of the lithosphere.

Group D pyroxenites—cpx-rich samples—are enriched in compatible elements such as Mg, Cr and Ni, and depleted in moderately incompatible elements such as Al, Ti and HREE. These compositions, as well as the calculated melt (Fig. 9c), indicate that their parental melts had a boninitic affinity, markedly different from the basaltic affinity of group B and C parental melts. The composition of group D parental melts may be partly explained by olivine- and melt-consuming reactions such as those inferred for the formation of secondary lherzolites in the fine-grained subdomain and group C websterites. This reaction can produce volatile, Mg-rich residual melts. However, its ability to generate the whole composition spectrum of refractory melts depends on the mass ratio of dissolved olivine to solidified melt. For moderate values of this ratio, the reaction does not account for some geochemical characteristics of group D parental melts, such as their low Ti and HREE contents. These characteristics may alternatively result from interaction of melts with refractory peridotites. This scenario is consistent with the proposal by Kelemen and coworkers that refractory peridotites and calc-alkaline magmas may be genetically related through olivine-forming melt–rock reaction in the upper mantle (Kelemen, 1990, 1995). However, the genetic relationships between the parental melts of group D, group C websterites and the refractory peridotites need to be further constrained by numerical modelling of melt–rock reactions and isotopic data.

Finally, the selective LILE enrichment and overall trace-element signature of group D dykes is similar to that observed in lithospheric mantle xenoliths affected by cryptic metasomatism (Fig. 11). This signature is generally ascribed to metasomatism by carbonatitic melts (Dautria *et al.*, 1992; Hauri *et al.*, 1993; Rudnick *et al.*, 1993). However, Bedini *et al.* (1997) have shown that it may be also accounted for by small volumes of asthenospheric basaltic melts migrating by porous flow under a lithospheric conductive thermal gradient. The selective LILE enrichment results from coupled chromatographic effects related to melt percolation (Navon & Stolper, 1987; Bodinier *et al.*, 1990) and source effects related to solid–melts reactions at decreasing melt mass (Godard *et al.*, 1995; Vernières *et al.*, 1997). In this model, the negative anomaly of Nb and Ta is explained by buffering of these elements by very small amounts of Ti-rich oxides (Bodinier *et al.*, 1996; Van der Wal & Bodinier, 1996). In Ronda, Van der Wal & Bodinier (1996) observed a similar trace-element signature in a harzburgite of the spinel tectonite domain collected at some distance (>1 km) from the recrystallization front. This observation may indicate that group D dykes tapped interstitial melts

percolating through the spinel tectonite domain. This domain was probably the coldest part of the massif during most of this late magmatic event recorded in Ronda.

CONCLUSIONS

The Ronda orogenic peridotite contains a wide diversity of mafic rocks, rarely encountered in other peridotite massifs. Our results indicate that most of this diversity was generated by multi-stage melt–rock reaction during the magma percolation event invoked for the development of the recrystallization front and the structural–geochemical zoning of the massif. The inferred magmatic event possibly occurred during the late mantle evolution of Ronda, and records thermal and compositional erosion of old subcontinental lithospheric mantle by upwelling asthenosphere in an extensional tectonic regime.

Garnet-bearing mafic layers (group A) are restricted to the spinel tectonite domain that represents the vestige of subcontinental lithospheric mantle preserved from thermal erosion. These layers are the oldest mafic rocks in Ronda. Os isotopes indicate that they have been isolated in the subcontinental lithospheric mantle for at least 1–2 billion years (Reisberg *et al.*, 1991). Their primary mineralogy and structure have been obscured by metamorphism and deformation. Their primary origin (recycled oceanic crust or cumulates in mantle conduits) remains an open question.

The other mafic rocks, mainly garnet-free pyroxenites occurring in the granular and plagioclase tectonite domains, record various stages of the magmatic event associated with different thermal stages of 'erosion' of thinned subcontinental lithosphere by upwelling asthenospheric mantle:

(a) Group B mafic layers were individualized during the earlier stages of this event, by open-system recrystallization of former group A layers. Their formation was coeval with the prograde evolution of the basaltic percolation domain, while the peridotites were partially molten and pervasively percolated by basaltic melts. Metasomatic replacement of group A layers by group B pyroxenites occurred at the recrystallization front—representing the permeability boundary of the basaltic porous flow domain—via melt-producing reactions. Major and trace-element chemistry of group B indicates that interstitial melts were tholeiitic at this stage, which is ascribed to the thermal 'climax' of lithospheric erosion by upwelling asthenosphere.

(b) Group C mafic layers were formed after the development of the recrystallization front, by near-solidus, melt-consuming reaction between interstitial magmas and peridotites. At this stage, the basaltic percolation domain was receding upon thermal relaxation. Basaltic porous flow was refracted and channelled against the permeability barrier represented by the base of the lithosphere. Group C layers materialize the successive positions of this barrier during the retrograde evolution of the basaltic porous flow domain in the granular peridotite and plagioclase tectonite domains. At this stage, interstitial melts incorporated a deep asthenospheric component and were transitional to alkaline in composition.

(c) Group D concordant mafic layers were formed by reaction of older mafic layers (groups A, B and C) with volatile-rich small melt fractions with a refractory (Mg-rich, Al-poor), calc-alkaline composition. This process took place during the waning stages of porous melt flow in Ronda, upon final cooling of the eroded lithosphere below the anhydrous solidus of peridotites. The origin of group D parental melts is not fully understood. They must somehow derive from melt fractions residual after olivine- and melt-consuming reactions such as those invoked for group C layers—as well as for the secondary lherzolites of the fine-granular layers; yet their composition may have been somewhat modified by further interaction with refractory peridotites (harzburgites and dunites). In contrast to channelled porous flow inferred for basaltic melts during thermal relaxation, the percolation of group D parental melts was pervasive and extensive throughout the Ronda massif. This feature is ascribed to the low viscosity and solidification temperature of these melts, because of their volatile-rich composition. They migrated beyond the recrystallization front and invaded most of the lithospheric domain which had not been affected by basaltic porous flow infiltration (i.e. the spinel tectonite domain). In this region, the small melt fractions probably encountered a significant thermal gradient along which they gradually solidified. This evolution is indicated by the LILE-enriched trace-element signature observed in group D intrusive dykes and harzburgites at some distance (>1 km) from the recrystallization front. In this domain, the last fractions of interstitial melts were tapped by cross-cutting dykes, indicating a final melt migration stage into cracks in colder lithospheric mantle.

ACKNOWLEDGEMENTS

C.J.G. is indebted to Professor Dr Fernando Gervilla, José Torres-Ruiz, and Puri Fenoll Hach-Ali for field, financial and technical support. Liliane Savoyant and Simone Pourtales are thanked for their assistance during ICP-MS work. This paper has benefited from discussions with Fernando Gervilla, Malika Remaïdi, Dirk Van der Wal, Martin Menzies, Fred Frey and Peter Kelemen. Fred Frey, Laurie Reisberg and Riccardo Vanucci provided thorough and thoughtful reviews. This study was undertaken by C.J.G. as a part of his Ph.D. project financed

by a graduate fellowship of the Spanish 'Ministerio de Educacion y Ciencia' (MEC). The completion of this work has been possible thanks to an MEC postdoctoral grant to C.J.G. (EX94-25995826) at WHOI. Other financial support came from Spanish CICYT projects (PB90-0274 and PB92-0922), 'Junta de Andalucia' research group 4028 (GIMPY) and the scientific co-operation programme 'PICS 275' between the 'Institut des Sciences de la Terre, de l'Eau et de l'Espace de Montpellier (UMR 5569)' and the 'Instituto Andaluz de Ciencias de la Tierra, Granada', funded by CNRS and Ministère des Affaires Etrangères (France), and CSIC (Spain).

REFERENCES

Allègre, C. J. & Turcotte, D. L. (1986). Implications of a two-component marble-cake mantle. *Nature* **263,** 123–127.

Bedini, R. M., Bodinier, J.-L., Dautria, J.-M. & Morten, L. (1997). Evolution of LILE-enriched small melt fractions in the lithospheric mantle: a case study from the East African Rift. *Earth and Planetary Science Letters* **153,** 67–83.

Bodinier, J.-L. (1989). Distribution des terres rares dans les massifs lherzolitiques de Lanzo et de l'Ariège. Ph.D. Thesis, Université de Montpellier II, 89 pp.

Bodinier, J.-L., Fabriès, J., Lorand, J.-P., Dostal, J. & Dupuy, C. (1987*a*). Geochemistry of amphibole pyroxenite veins from the Lherz and Freychinède ultramafic bodies (Ariège, French Pyrénées). *Bulletin de Minéralogie* **110,** 345–358.

Bodinier, J.-L., Guiraud, M., Fabriès, J., Dostal, J. & Dupuy, C. (1987*b*). Petrogenesis of layered pyroxenites from the Lherz, Freychinède and Prades ultramafic bodies (Ariège, French Pyrénées). *Geochimica et Cosmochimica Acta* **51,** 279–290.

Bodinier, J.-L., Dupuy, C. & Dostal, J. (1988). Geochemistry and petrogenesis of Eastern Pyrenean peridotites. *Geochimica et Cosmochimica Acta* **52,** 2893–2907.

Bodinier, J.-L., Vasseur, G., Vernières, J., Dupuy, C. & Fabriès, J. (1990). Mechanisms of mantle metasomatism: geochemical evidence from the Lherz orogenic peridotite. *Journal of Petrology* **31,** 597–628.

Bodinier, J. L., Merlet, C., Bedini, R. M., Simien, F., Remaidi, M. & Garrido, C. J. (1996). Distribution of niobium, tantalum, and other highly incompatible trace elements in the lithospheric mantle: the spinel paradox. *Geochimica et Cosmochimica Acta* **60,** 545–550.

Boudier, F. & Nicolas, A. (1995). Nature of the Moho transition zone in the Oman ophiolite. *Journal of Petrology* **36,** 777–796.

Burg, J.-P., Bodinier, J.-L., Chaudhry, S., Hussain, S. & Dawood, H. (1998). Infra-arc mantle–crust transition and infra-arc mantle diapirs in the Kohistan Complex (Pakistani Himalayas). Petro-structural evidence. *Terra Nova* **10,** 74–80.

Cameron, W. E. (1989). Contrasting boninite–tholeiite associations from New Caledonia. In: Crawford, J. E. (ed.) *Boninites and Related Rocks*. London: Unwin Hyman, pp. 314–354.

Cameron, W. E., McCulloch, M. T. & Walker, D. A. (1983). Boninite petrogenesis: chemical and Nd–Sr isotopic constraints. *Earth and Planetary Science Letters* **65,** 75–89.

Conquéré, F. (1971). Les pyroxénolites à amphibole et les amphibolites associées aux lherzolites du gisement de Lherz (Ariège, France): un exemple du rôle de l'eau au cours de la cristallisation fractionnée des liquides issus de la fusion partielle de lherzolites. *Contributions to Mineralogy and Petrology* **33,** 32–61.

Conquéré, F. (1977). Pétrologie des pyroxénites litées dans les complexes ultramafiques de l'Ariège (France) et autres gisements de lherzolite à spinelle. I. Composition minéralogiques et chimiques, évolution des conditions d'équilibre des pyroxénites. *Bulletin de la Société Française de Minéralogie et de Cristallographie* **160,** 42–80.

Crawford, A. J. (ed.) (1989). *Boninites and Related Rocks*. London: Unwin Hyman.

Dautria, J. M., Dupuy, C., Takherist, D. & Dostal, J. (1992). Carbonate metasomatism in the lithospheric mantle: peridotite xenoliths from a melilititic district of the Sahara basin. *Contributions to Mineralogy and Petrology* **111,** 37–52.

Davies, G. R., Nixon, P. H., Pearson, D. G. & Obata, M. (1993). Tectonic implications of graphitized diamonds from the Ronda peridotite massif, southern Spain. *Geology* **21,** 471–474.

DeBari, S. M. & Sleep, N. H. (1991). High-Mg, low-Al bulk composition of the Talkeetna island arc, Alaska: implications for primary magmas and the nature of the arc crust. *Geological Society of America Bulletin* **103,** 37–47.

Dickey, J. S., Jr (1970). Partial fusion products in alpine-type peridotites: Serrania De La Ronda and other examples. *Mineralogical Society of America, Special Papers* **3,** 33–49.

Downes, H., Bodinier, J. L., Thirwall, M. F., Lorand, J. P. & Fabriès, J. (1991). REE and Sr–Nd isotopic geochemistry of eastern Pyrenean peridotite massifs: sub-continental lithospheric mantle modified by continental magmatism. *Journal of Petrology* (Special Lherzolites Issue), 97–115.

Fabriès, J., Bodinier, J.-L., Dupuy, C., Lorand, J.-P. & Benkerrou, C. (1989). Evidence for modal metasomatism in the orogenic spinel lherzolite body from Caussou (Northeastern Pyrenees, France). *Journal of Petrology* **30,** 199–228.

Frey, F. A. (1980). The origin of pyroxenites and garnet pyroxenites from Salt Lake Crater, Oahu, Hawaii: trace element evidence. *American Journal of Science* **280-A,** 427–449.

Frey, F. A. & Prinz, M. (1978). Ultramafic inclusions from San Carlos, Arizona: petrologic and geochemical data bearing on their petrogenesis. *Earth and Planetary Science Letters* **38,** 129–176.

Frey, F. A., Suen, C. J. & Stockman, H. W. (1985). The Ronda high temperature peridotite: geochemistry and petrogenesis. *Geochimica et Cosmochimica Acta* **49,** 2469–2491.

Garrido, C. J. (1995). Estudio geoquímico de las capas máficas del mazico ultramáfico de Ronda (Cordillera Bética, Sur de España). Ph.D. Thesis, Universidad de Granada, 273 pp.

Garrido, C. J. & Bodinier, J. L. (1998). Distribution of trace elements in minerals from anhydrous spinel peridotites and websterites from the Ronda peridotite: implications for the nature of LILE, REE and HFSE reservoirs in the subcontinental lithospheric mantle. *Mineralogical Magazine* **62A,** 498–499.

Garrido, C. J., Remaïdi, M., Bodinier, J. L., Gervilla, F., Torres-Ruiz, J. & Fenoll, P. (1993). Replacive pyroxenites in the Ronda orogenic lherzolite: evidence for km-scale percolation of calc-alkaline melts in the upper mantle. *Terra Abstracts* **68,** 477.

Gervilla, F. & Remaïdi, M. (1993). Field trip to the Ronda ultramafic massif: an example of asthenosphere–lithosphere interaction? *Ofioliti* **18,** 21–35.

Godard, M., Bodinier, J.-L. & Vasseur, G. (1995). Effects of mineralogical reactions to trace element redistributions in mantle rocks during percolation processes: a chromatographic approach. *Earth and Planetary Science Letters* **133,** 449–461.

Griffin, W. L., Wass, S. Y. & Hollis, J. D. (1985). Ultramafic xenoliths from Bullenmerri and Gnotuk maars, Victoria, Australia: petrology of a crust–mantle transition. *Journal of Petrology* **25,** 53–87.

Hamelin, B. & Allègre, C. J. (1988). Lead isotope study of orogenic lherzolite massifs. *Earth and Planetary Science Letters* **91,** 117–131.

Hart, S. R. & Dunn, T. (1993). Experimental cpx/melt partitioning of 24 trace elements. *Contributions to Mineralogy and Petrology* **113,** 1–8.

Hauri, E., Shimizu, N., Dieu, J. J. & Hart, S. R. (1993). Evidence for hotspot-related carbonatite metasomatism in the oceanic upper mantle. *Nature* **365,** 221–227.

Hauri, E. H. (1996). Major element variability in the Hawaiian mantle plume. *Nature* **382,** 415–419.

Hickey, R. L. & Frey, F. A. (1982). Geochemical characteristics of boninite series volcanics: implications for their source. *Geochimica et Cosmochimica Acta* **46,** 2099–2115.

Hirschmann, M. M. & Stolper, E. M. (1996). A possible role for garnet pyroxenite in the origin of the 'garnet signature' in MORB. *Contributions to Mineralogy and Petrology* **124,** 185–208.

Ionov, D. A., Savoyant, L. & Dupuy, C. (1992). Application of the ICP-MS technique to trace-element analysis of peridotites and their minerals. *Geostandards Newsletters* **16,** 311–315.

Irving, A. J. (1980). Petrology and geochemistry of composite ultramafic xenoliths in alkaline basalts and implications for magmatic processes within the mantle. *American Journal of Science* **280-A,** 389–426.

Kelemen, P. B. (1986). Assimilation of ultramafic rocks in subduction-related magmatic arcs. *Journal of Geology* **94,** 829–843.

Kelemen, P. B. (1990). Reaction between ultramafic rock and fractionating basaltic magma I: phase relations, the origin of calc-alkaline magma series, and the formation of discordant dunite. *Journal of Petrology* **31,** 51–98.

Kelemen, P. B. (1995). Genesis of high Mg andesites and the continental crust. *Contributions to Mineralogy and Petrology* **120,** 1–19.

Kelemen, P. B. & Dick, H. J. B. (1995). Focused melt flow and localized deformation in the upper mantle: juxtaposition of replacive dunite and ductile shear zones in the Josephine peridotites, SW Oregon. *Journal of Geophysical Research* **100,** 423–438.

Kelemen, P. B., Johnson, K. T. M., Kinzler, R. J. & Irving, A. J. (1989). High field strength element depletions in arc basalts due to mantle–magma interaction. *Nature* **345,** 521–524.

Kelemen, P. B., Shimizu, N. & Dunn, T. (1993). Relative depletion of niobium in some arc magmas and the continental crust: partitioning of K, Nb, La and Ce during melt/rock reaction in the upper mantle. *Earth and Planetary Science Letters* **120,** 111–134.

Kornprobst, J. (1969). Le massif ultrabasique de Beni Bouchera (Rif Internne, Maroc): étude des péridotites de haute témperature et de haute pression, et des pyroxénolites a grènat ou sans grènat, qui leur sont associées. *Contributions to Mineralogy and Petrology* **23,** 283–322.

Kornprobst, J. (1970). Les péridotites et les pyroxénolites du massif ultrabasique des Beni Bouchera: une étude expérimentale entre 1100 et 1550°C, sous 15 à 30 kilobars de pression sèche. *Contributions to Mineralogy and Petrology* **29,** 290–309.

Kornprobst, J., Piboule, M. & Tabit, A. (1987). Diversité des clinopyroxénites à grenat associées aux massifs ultramafiques orogéniques: éclogites, ariégites, griquaites et grospydites; une discussion. *Bulletin de la Société Géologique de France* **8 (III),** 345–351.

Kornprobst, J., Piboule, M., Roden, M. & Tabit, A. (1990). Corundum-bearing garnet clinopyroxenites at Beni Bousera (Morocco): original plagioclase-rich gabbros recrystallized at depth within the mantle? *Journal of Petrology* **31,** 717–745.

Kumar, N., Reisberg, L. & Zindler, A. (1996). A major and trace element and strontium, neodymium, and osmium isotopic study of a thick pyroxenite layer from the Beni Bousera ultramafic complex of northern Morocco. *Geochimica et Cosmochimica Acta* **60,** 1429–1444.

Loubet, M. & Allègre, C. J. (1982). Trace elements in orogenic lherzolites reveal the complex history of the upper mantle. *Nature* **298,** 809–814.

Mattie, P. D., Condie, K. C., Selverstone, J. & Kyle, P. R. (1997). Origin of the continental crust in the Colorado Plateau: geochemical evidence from mafic xenoliths from the Navajo Volcanic Field, Southwestern USA. *Geochimica et Cosmochimica Acta* **61,** 2007–2021.

McKenzie, D. (1989). Some remarks on the movement of small melt fractions in the mantle. *Earth and Planetary Science Letters* **95,** 53–72.

Navon, O. & Stolper, E. (1987). Geochemical consequence of melt percolation: the upper mantle as a chromatographic column. *Journal of Geology* **95,** 285–307.

Obata, M. (1980). The Ronda peridotite: garnet-, spinel-, and plagioclase-lherzolite facies and the *P–T* trajectories of a high-temperature mantle intrusion. *Journal of Petrology* **21,** 533–572.

Obata, M. & Nagahara, N. (1987). Layering of alpine-type peridotite and the segregation of partial melt in the upper mantle. *Journal of Geophysical Research* **92,** 3467–3474.

Obata, M., Suen, C. J. & Dickey, J. S. J. (1980). The origin of mafic layers in the Ronda high-temperature peridotite intrusion, S. Spain: an evidence of partial fusion and fractional crystallization in the upper mantle. *Colloques Internationaux du CNRS* **272** ('Les Orogènes'), 257–268.

O'Hara, M. J. & Yoder, H. S., Jr (1967). Formation and fractionation of basic magmas at high pressures. *Scottish Journal of Geology* **3,** 67–117.

Orberger, B., Lorand, J. P., Girardeau, J., Mercier, J. C. C. & Pitragool, S. (1995). Petrogenesis of ultramafic rocks and associated chromitites in the Nan Uttaradit ophiolite, Northern Thailand. *Lithos* **35,** 153–182.

Pearson, D. G., Davies, G. R., Nixon, P. H. & Milledge, H. J. (1989). Graphitized diamonds from a peridotite massif in Morocco and implications for anomalous diamond occurrences. *Nature* **338,** 60–62.

Pearson, D. G., Davies, G. R., Nixon, P. H., Greenwood, P. B. & Mattey, D. P. (1991). Oxygen isotope evidence for the origin of pyroxenites in the Beni Bousera peridotite massif, north Morocco: derivation from subducted oceanic lithosphere. *Earth and Planetary Science Letters* **102,** 289–301.

Pearson, D. G., Davies, G. R. & Nixon, P. H. (1993). Geochemical constraints on the petrogenesis of diamond facies pyroxenites from the Beni Bousera peridotite massif, North Morocco. *Journal of Petrology* **34,** 125–172.

Platt, J. P. & Vissers, R. L. M. (1989). Extensional collapse of thickened continental lithosphere: a working hypothesis for the Alboran Sea and Gibraltar Arc. *Geology* **17,** 540–543.

Polvé, M. & Allègre, C. J. (1980). Orogenic lherzolite complexes studied by ^{87}Rb–^{87}Sr: a clue to understand the mantle convection processes? *Earth and Planetary Science Letters* **51,** 71–93.

Prinzhofer, A., Lewin, E. & Allègre, C. J. (1989). Stochastic melting of the marble cake mantle: evidence from local study of the East Pacific Ridge at 12° 50′. *Earth and Planetary Science Letters* **92,** 189–206.

Rampone, E., Bottazzi, P. & Ottolini, L. (1991). Complementary Ti and Zr anomalies in orthopyroxene and clinopyroxene from mantle peridotites. *Nature* **354,** 518–520.

Reisberg, L. & Lorand, J.-P. (1995). Longevity of sub-continental mantle lithosphere from osmium isotope systematic in orogenic peridotite massifs. *Nature* **376,** 159–162.

Reisberg, L. C., Allègre, C. J. & Luck, J. M. (1991). The Re–Os systematic of the Ronda Ultramafic Complex of southern Spain. *Earth and Planetary Science Letters* **105,** 196–213.

Remaïdi, M. (1993). Étude pétrologique et géochimique d'une association péridotites refractaires–pyroxenites dans le Massif de Ronda (Espagne). Ph.D. Thesis, Université de Montpellier II, 437 pp.

Rogers, G. & Saunders, A. D. (1989). Magnesian andesites from Mexico, Chile and the Aleutian Island: implications for magmatism associated with ridge–trench collision. In: Crawford, J. E. (ed.) *Boninites and Related Rocks*. London: Unwin Hyman, pp. 417–446.

Rudnick, R. L. & Fountain, D. M. (1995). Nature and composition of the continental crust: a lower crustal perspective. *Reviews of Geophysics* **33,** 267–309.

Rudnick, R. L., McDonough, W. F. & Chappell, B. W. (1993). Carbonatite metasomatism in the northern Tanzanian mantle: petrographic and geochemical characteristics. *Earth and Planetary Science Letters* **114,** 463–475.

Shervais, J. W. (1979). Thermal emplacement model for the alpine lherzolite massif at Balmuccia, Italy. *Journal of Petrology* **20,** 795–820.

Sparks, D. W. & Parmentier, E. M. (1991). Melt extraction from the mantle beneath spreading centers. *Earth and Planetary Science Letters* **105,** 368–377.

Spiegelman, M. (1993). Physics of melt extraction: theory, implications and applications. *Philosophical Transactions of the Royal Society of London, Series A* **342,** 23–41.

Suen, C. J. & Frey, F. A. (1987). Origins of the mafic and ultramafic rocks in the Ronda peridotite. *Earth and Planetary Science Letters* **85,** 183–202.

Sun, S.-S. & McDonough, W. F. (1989). Chemical and isotopic systematics of oceanic basalts: implications for mantle composition and processes. In: Saunders, A. D. & Norry, M. J. (eds) *Magmatism in the Ocean Basins. Geological Society, London, Special Publication* **42,** 313–345.

Sun, S.-S., Hanson, G. N. & Sharskin, A. Y. (1979). Geochemical characteristics of mid-ocean ridge basalts. *Earth and Planetary Science Letters* **44,** 119–138.

Tubia, J. M. (1994). The Ronda peridotites (Los Reales nappe): an example of the relationship between lithospheric thickening by oblique tectonics and late extensional deformation within the Betic Cordillera (Spain). *Tectonophysics* **238,** 381–398.

Tubia, J. M. & Cuevas, J. (1986). High-temperature emplacement of the Los Reales peridotite nappe (Betic Cordillera, Spain). *Journal of Structural Geology* **8,** 473–482.

Van der Wal, D. & Bodinier, J. L. (1996). Origin of the recrystallisation front in the Ronda peridotite by km-scale pervasive porous melt flow. *Contributions to Mineralogy and Petrology* **122,** 387–405.

Van der Wal, D. & Vissers, R. L. M. (1993). Uplift and emplacement of upper mantle rocks in the western Mediterranean. *Geology* **21,** 1119–1121.

Van der Wal, D. & Vissers, R. L. M. (1996). Structural petrology of the Ronda peridotite, SW Spain: deformation history. *Journal of Petrology* **37,** 23–43.

Varfalvy, V., Herbert, R. & Bédard, J. H. (1996). Interactions between melt and upper-mantle peridotites in the North Arm Mountain Massif, Bay of Islands Ophiolite, Newfoundland, Canada: implications for the genesis of boninites and related magmas. *Chemical Geology* **129,** 71–90.

Vernières, J., Godard, M. & Bodinier, J. L. (1997). A plate model for the simulation of trace-element fractionation during partial melting and magma transport in the Earth's upper mantle. *Journal of Geophysical Research* **102,** 24771–24784.

Vissers, R. L. M., Platt, J. P. & Van der Wal, D. (1995). Late orogenic extension of the Betic Cordillera and the Alboran domain: a lithospheric view. *Tectonics* **14,** 786–803.

Watson, E. B. & Brenan, J. M. (1987). Fluids in the lithosphere. 1: Experimentally-determined wetting characteristics of CO_2–H_2O fluids and their implications for fluid transport, host-rock physical properties, and fluid inclusion formation. *Earth and Planetary Science Letters* **85,** 497–515.

Wilshire, H. G. & Shervais, J. W. (1975). Al-augite and Cr-diopside ultramafic xenoliths in basaltic rocks from western United States. *Physics and Chemistry of the Earth* **9,** 257–272.

Wilshire, H. G., Nielson, J. E., Pike, J. E. N., Meyer, C. E. & Schwarzman, E. C. (1980). Amphibole-rich veins in lherzolite xenoliths, Dish Hill and Deadman Lake, California. *American Journal of Science* **280A,** 576–593.

Xu, Y. G., Menzies, M. A., Bodinier, J.-L., Bedini, R. M., Vroon, P. & Mercier, J.-C. C. (1998). Melt percolation–reaction at the lithosphere–plume boundary: evidence from poikiloblastic peridotite xenoliths from Borée (Massif Central, France). *Contributions to Mineralogy and Petrology* **131,** 65–84.

Yoder, H. S. & Tilley, C.E. (1962). Origin of basalt magmas: an experimental study of natural and synthetic rock systems. *Journal of Petrology* **3,** 342–532.

Zindler, A., Staudigel, H., Hart, S. R., Endres, R. & Goldstein, S. (1983). Nd and Sr isotopic study of a mafic layer from Ronda ultramafic complex. *Nature* **304,** 226–230.